Glomerular Elasticity and Gene Expression Patterns Define Two Phases of Alport Nephropathy

Joonho Yoon*[1], Zhenan Liu*[1], Matthew Alaba[5], Leslie A. Bruggeman[6], Paul A. Janmey[7], Carlos A. Arana[2], Oluwatoyosi Ayenuyo[8], Isabela Medeiros[8], Sean Eddy[5], Matthias Kretzler[5], Joel M. Henderson[8], Abhijit Naik[5], Audrey N. Chang[1,4], R. Tyler Miller[1,3,4, #]

[1]Department of Internal Medicine, University of Texas Southwestern Medical Center, Dallas Texas, USA

[2]Department of Immunology, The University of Texas Southwestern Medical Center, Dallas, Texas, 75390, USA

[3]Medicine Service, VA North Texas Health Care System, Dallas, TX, USA.

[4]Pak Center for Mineral Metabolism and Clinical Research, UTSW Medical Center, Dallas Texas, USA

[5]Department of Internal Medicine, University of Michigan, Ann Arbor, Michigan, USA.

[6]Department of Inflammation & Immunity, Lerner Research Institute, Cleveland Clinic, Cleveland, Ohio, USA

[7]Department of Physiology and Institute for Medicine and Engineering, University of Pennsylvania, Philadelphia, PA, 19104, USA.

[8]Department of Pathology and Laboratory Medicine, Boston University Chobanian & Avedisian School of Medicine and Boston Medical Center, Boston, MA, USA

[#]Corresponding author- R. Tyler Miller, Nephrology, 8856, 5323 Harry Hines Blvd, Dallas TX 75390, 214-648-7214, tyler.miller@utsouthwestern.edu

The authors have declared that no conflict of interest exists.

*Co-first author. These authors contributed equally to this work.

Abstract.

Rationale- The causes of podocyte injury in collagen IV nephropathies are not fully defined.

Objectives- We characterized renal function, structural and biophysical properties of glomerular capillaries and podocytes, and renal gene expression in *Col4a3*$^{-/-}$ mice over the 8-month course of disease and treated Col4α3$^{-/-}$ mice with TUDCA to test for a role of ER stress.

Findings- *Col4a3*$^{-/-}$ mice develop proteinuria and reduced renal function at 4 – 5 months, but glomerular capillaries become deformable, with podocyte injury evident at 3 months. Glomeruli are maximally deformable at 4 months with 40% podocyte loss, and then stiffen progressively. In parallel, kidneys become increasingly fibrotic with proteinuria and inflammatory infiltrates as renal failure progresses. Bulk RNAseq at 2 and 4 months shows minimal increases in expression of genes related to matrix, cytokine and chemokine signaling, and cell injury with significant increases at 7 months when loss of differentiated gene expression also occurs. TUDCA suppressed glomerular and renal injury, and reversed disease-associated change in gene expression. Comparison of bulk RNAseq data from 7 Mo Col4α3$^{-/-}$ mice with a NEPTUNE FSGS population revealed shared gene expression changes related to proteinuria and activation of the TNF pathway.

Conclusions- *Col4a3*$^{-/-}$ nephropathy progresses in two phases, before overt proteinuria with early podocyte injury and loss, and later with overt proteinuria, progressive fibrosis, and increased expression of interleukins, cytokines, and chemokines including TNF pathway activation. Suppression of renal injury by TUDCA implicates ER stress as a disease mechanism. The Alport mouse model shares renal injury pathways with a NEPTUNE FSGS population.

Introduction.

Many glomerular diseases including Alport syndrome, caused by mutations in *COL4A3,4, or 5,* focal sclerosing glomerulonephritis (FSGS), or IgA Nephropathy (IgAN) begin with podocyte injury that is followed by varying degrees of proteinuria, hematuria, and tubulo-interstitial damage. The first evidence of podocyte injury is disruption of foot process architecture, foot process effacement, with their flattening, spreading, and loss of slit diaphragms. Further injury leads to detachment, loss of podocytes in the urine, and at some point, irreversible glomerular damage associated with tubulo-interstitial fibrosis and progression to end stage renal disease. The mechanisms that cause early podocyte injury and related changes in gene expression are not fully defined. Additionally, *COL4A3,4,5* mutations are important beyond Alport syndrome because the heterozygous state is found increasingly in other more common glomerular diseases including FSGS and IgA Nephropathy(1). Thin Basement Membrane Nephropathy (TBMN), caused by heterozygous *COL4A3,4, or 5* mutations is increasingly recognized as a cause of chronic kidney disease(1-4).

Podocytes accommodate traction and shear forces and contribute to a specific biophysical environment for glomerular capillaries, all of which depend on the podocytes' unique cytoskeletal structure. That structure and cell function are maintained by factors that include attachment to the GBM, lateral attachment of foot processes to foot processes of neighboring podocytes, Ca fluxes, various signaling pathways, and mechanical environment (elasticity of the GBM, shear forces, and stretch)(5-12). In rats, 5/6 renal reduction causes glomerular capillary dilation to prevent increased shear stress(13). In acute and chronic glomerular injury models including Alport syndrome, protamine, HIV nephropathy, ischemia and ischemia-reperfusion injury, the deformability of glomerular capillaries increases as a result of podocyte injury(10, 11, 14-16). Recent intravital imaging studies show distension of glomerular capillaries and aneurisms in glomeruli from *Col4a5*$^{-/-}$ mice at an early stage of disease, indicating increased deformability and reduced structural integrity of these capillaries at a time of accelerated podocyte loss(17-19). Loss of podocytes reflects abnormal podocyte structure with reduced adhesion that may occur due to primary podocyte injury or abnormal matrix, and these two factors may be interrelated(7, 8, 10). Foot process effacement may represent a compensatory mechanism to maintain podocyte attachment to the glomerulus(20).

We used the C57BL/6J *Col4a3*$^{-/-}$ mouse model of Alport syndrome, a disease of glomerular origin, to study early steps in podocyte injury. This model retains many essential characteristics of the human disease, including accelerated podocyte loss, and has an 8 month time course allowing better time resolution of disease development and progression than other mouse strains(21-23). The abnormal GBM could injure podocytes through abnormal physical properties or abnormal signaling due to chemical differences in the normal compared to the Alport GBM(8, 24). Podocytes that produce COL4α3, 4, and 5 could be injured by accumulation of the mutant or misfolded collagen molecules with activation of the unfolded protein response (UPR, ER stress) and additional cell-specific remodeling pathways (25). Finally, abnormal glomerular capillary mechanics caused by disordered cytoskeletal structure could contribute to progressive podocyte injury though increased susceptibility to mechanical injury.

To distinguish among these injury mechanisms, we treated one group of *Col4a3*$^{-/-}$ mice with TauroUrsoDeoxyCholic Acid, 3α,7β-Dihydroxy-5β-cholanoyltaurine (TUDCA, *Col4a3*$^{-/-}$-T), a compound that functions as a chemical chaperone and that protects cells from UPR-mediated injury or death(26-29). We analyzed renal function, glomerular capillary elasticity, structure, and bulk renal RNA expression over the course of disease. We find that Alport syndrome progresses in two phases, the first characterized by increasing capillary deformability and podocyte loss, and the second characterized by increasing proteinuria, decreasing renal excretory function, decreasing glomerular elasticity, and increasing expression of genes related to fibrosis and inflammation. TUDCA treatment suppressed the *Col4a3*$^{-/-}$ phenotype.

Results.

Increased glomerular capillary deformability precedes proteinuria and increased creatinine in Col4α3$^{-/-}$ mice. We studied the *Col4a3* mutant in the C57/Bl6 background to characterize the course of Alport nephropathy and glomerular capillary elasticity, a biophysical parameter that is poorly understood. An advantage of this mouse strain is its relatively long disease course with the opportunity for accurate timing of events. Although referred to as a *Col4a3* knockout mouse, in fact the mutation is a truncation deleting the Co4α3$^{-/-}$ NC1 domain so that mRNA and protein presumably representing the 7S and collagenous domains are expressed (**Figure S1**)(21-23). We compared renal function and glomerular capillary elasticity, a marker of podocyte structural integrity, in *Col4a3*$^{-/-}$ mice and control littermates from 2 to 8 months of age. We measured serum creatinine (**Figure 1A**) and urine Albumin/Creatinine Ratio (ACR) (**Figure 1B**) beginning at 2 months of age. From 4 months, creatinine increased but did not reach statistical significance until 6 months and reached a maximum value of 61 µM at 8 months. Similarly, urine ACR increased from 0.82 at 3 months (vs 0.14 in Control) and 3.51 at 4 months (Control 0.059) to 122 at 8 months. Over this time course, the serum creatine and urine ACR values in the control mice did not change significantly.

Past work using models of acute and chronic kidney diseases, showed that glomerular capillary elasticity reflects the state of podocyte cytoskeletal structure and that with podocyte injury, capillaries have increased deformability (10, 11, 16). We measured glomerular elasticity (Young's modulus, E) in the control and *Col4a3*$^{-/-}$ mice from 2 to 8 months of age using micro-indentation (**Figure 1C**)(30). The values of E for both the control and *Col4a3*$^{-/-}$ mice were indistinguishable at 2 months (both 2.2 ± 0.2 kPa) and the values for the control mice remained essentially unchanged from 2 to 8 months. However, in the *Col4a3*$^{-/-}$ mice, the E values for glomeruli began to decrease at 3 months (1.85±0.09 kPa) and reached a minimum (1.56 ± 0.3 kPa) at 4 months of age. E then increased to values significantly greater than control by 7 months, reaching a maximum at 8 months (2.7 ± 0.1 kPa). These directionally opposite changes in elasticity early and late in disease signify distinctly different structural and functional properties of glomerular capillaries(10, 11, 31, 32). The early time point at which reduced glomerular E appears, before increases in serum creatine and with a minor increase in urine ACR, indicates that podocyte injury begins early in the course of renal disease, and is sufficiently severe to affect overall glomerular capillary mechanical properties.

To assess gene expression patterns in the *Col4a3*$^{-/-}$ kidneys compared to WT over the course of renal disease, we performed bulk RNAseq of renal cortex at 2, 4, and 7 months. Upregulated pathways include those involved in extracellular matrix organization, chronic inflammation and fibrosis, innate immunity, and cytokine signaling Figure (S2). Upstream regulator analysis shows that these processes are driven by cytokines including Ifn-γ, TGF-β1, IL-1β, TNF, IL-6, and IGF1-activated pathways. We identified 1346 differentially expressed genes (DEGs) between WT and *Col4a3*$^{-/-}$ (KO) mice. **Figure 1D shows** a heatmap with expression of selected genes grouped vertically by function, and from 2 to 7 months horizontally with each column representing a separate mouse. The gene expression patterns change as a whole over time, but not dramatically in the 2-4 month period, reflecting the patterns in renal function and histology (see below). However, at 7 months, reflecting disease progression from 4 to 7 months, the changes are more dramatic, and all shown are statistically significant. The expression levels of renal injury markers, HAVCR1 (Kim1) and Lcn2 (NGAL) are increased at each time point compared to WT, but most dramatically at 7 months when most changes are statistically significant. EGF expression decreases minimally until 7 months when it decreases by half. Similarly, the expression of several kidney-specific transporters, Slc2a5 (Glut 5), Slc26a4 (Pendrin), Slc22a7 (OAT2), Aqp4, Slc16a4 (monocarboxylic acid transporter), and Slc12a3 (NCC) decrease significantly only at 7 months. The expression of genes involved in inflammation and fibrosis (C3, TNF, Tlr8, Thrombospondin, Ltbp2, Inhibin, Col1a1, Col1a2, Col3a1, Lox (Lysyl oxidase) as well as numerous cytokines, interleukins, and chemokines all increase most dramatically at 7 months (**Supplemental Tables 1A and B**).

In the WT vs Col4α3$^{-/-}$ comparison, expression of the podocyte-associated genes, Nphs1 (2.3 X), Nphs2 (2.1 X), Pdpn (2.25 X), Fat1(1.5 X) and Synpo (1.9 X) were increased in the Col4α3$^{-/-}$ mice at 4 Mo**,** compared to WT, while WT1, Cd2ap, and Actn4 were not differentially expressed. This pattern of gene expression and that of other genes involved in hypertrophy including increased Cdkn1c, IGF1, IGFBP2, and markers of mTOR and AMPK signaling (Ribosomal protein S6 kinase, Eukaryotic Translation Initiation Factor 4E Binding Protein 1 (Eif4ebp1), casein kinase, NUAK kinase, Lamtor, Shroom3, PTEN, and Pparg genes), suggest that Col4α3$^{-/-}$ podocytes are undergoing hypertrophy at this time point(33, 34).

Gene Ontology (GO) analysis shows that Inflammation is the principal response in KO kidneys, is detected as early as 2 months, and becomes prominent at 7 months. Using the IC6 gene list associated with proteinuria and the GO and KEGG pathway and interactome analyses at 2, 4, and 7 months, we identified several interaction nodes, Epithelium Development, ECM-receptor interaction, Skin development, Keratinocyte differentiation, PI3K-Akt signaling pathway, Estrogen signaling pathway, Negative regulation of signaling, Staphylococcus aureus infection, and IL-17 signaling (**Supplemental Figure S3**)(35). This pattern of gene expression and interactions indicates that in the Col4α3$^{-/-}$ mice, renal epithelial cell growth, matrix remodeling, and cell adhesion are activated compared to the WT mice. The involvement of IL-17 signaling is interesting given its involvement in innate immunity, response to bacterial and fungal pathogens, development of tissue-resident immune cells, important role in maintenance of epithelial barrier function, and tissue repair(36, 37).

To identify early gene expression changes related to progressive renal disease, we used a two-stage analysis method. First, we identified differentially expressed genes at 7 months using hypothesis-driven selections based on functional characteristics, direction, and magnitude of change **(Supplemental Figure S4A)**. We then focused our analysis of these genes at the two-month time point to investigate early gene changes. This group of genes (Tnc, Col4a3, Lox, Scube1, MMP2 and TIMP1) were enriched for Biological Process modules Extracellular Matrix organization (GO:0030198) and a sub-set of those genes (Scube1, MMP2, and Timp1) identified the extracellular matrix disassembly module (GO:0022617). This subset also identified the cellular component disassembly module (GO:0022411) **(Supplemental Figure S4B)**. In the Reactome analysis, a group of eight genes (Col4α3, Lox, Scube1, MMP2, Timp1, Lcn2, Vim, and Cxcl1) appear in a network of interactions among Extracellular Matrix Organization (R-HAS-1474244), Signaling by Interleukins (R-HAS-449147), and Interleukin-4 and Interleukin 13 signaling (R-HAS-6785807) (**Supplemental Figure S4C**). IL-4 and IL-13 have similar functions, are involved in wound healing, are produced by B cells, and signal through the JAK-Stat6 pathway(38, 39). Antibody-independent, and antigen-specific B cell production of IL-4 production in mouse glomeruli is sufficient to produce foot process effacement in mice, and IL-4 signaling is evident in glomeruli of some patients with minimal change disease(39, 40). These results indicate that processes that begin at 2 months in Col4α3$^{-/-}$ mice involving IL-4 and IL-13 signaling are early evidence of an immune component of renal disease in this Alport model. These results support the phenotypic data that show that renal injury is subtle up to 4 months but

progresses dramatically and potentially irreversibly in the 4 – 7 month period. They further indicate that identifying disease mechanisms in the 0 – 4 month period may offer improved opportunities for intervention.

Evidence for unfolded protein pathway activation in Col4α3$^{-/-}$ podocytes. Podocytes, the cells that provide mechanical support for glomerular capillaries, determine the elastic properties of glomerular capillaries, and form the slit diaphragms, also produce and secrete the Col4α3,4,5 heterotrimer for the GBM(41). With loss-of-function mutations in any one of these proteins, podocytes must contend with inadequately processed collagen(25, 42, 43). Cells compensate for excess or misfolded protein by upregulating pathways that can improve folding and/or protein degradation including Bip (HSPA5), Xbp1s (Xbp1) and CHOP (DDIT3). We imaged WT and Col4α3$^{-/-}$ mouse cortex with confocal microscopy and found increased Bip expression in glomerular podocytes (**Figure 2A**). The levels of Bip and Xbp1s, protein and mRNA are increased in conditionally immortalized Col4α3$^{-/-}$ podocytes compared to their WT counterparts (**Figure 2B**). WT cultured podocytes increase expression of Bip, Xbp1s, and CHOP in response to Tunicamycin, an agent that induces UPR, and the expression is reduced in a dose-dependent manner by treatment with TUDCA(26, 27, 29) (**Figure 2D**). For these reasons, we propose that an early step in podocyte injury could be UPR activation with disruption of normal protein processing and degradation. If the effects of UPR activation and podocyte remodeling could be suppressed, podocyte injury could be less severe or develop more slowly.

TUDCA treatment slows progression of renal disease in Col4α3$^{-/-}$ mice. Although ER stress activation due to Col IV misfolding was found in cultured cell-based systems, a mouse model, and human skin fibroblasts from Alport patients, protection from renal disease by inhibition of ER stress has not been demonstrated *in vivo*(25, 44). We tested the hypothesis that if collagen misfolding is the basis for podocyte injury in the Col4α3$^{-/-}$ mice, suppression of ER stress would preserve renal function. Col4α3$^{-/-}$ mice were fed 0.8% TUDCA-incorporated into mouse chow from the time of weaning, 21 - 25 days old, 3 – 4 months before they developed proteinuria, and until sacrifice(45). Normal littermates served as controls. We measured the effects of TUDCA treatment on Col4α3$^{-/-}$ mouse serum creatinine (**Figure 3A**), urine ACR (**Figure 3B**), and the Young's elastic modulus (E) of glomeruli (**Figure 3C**) at 4 and 7 months, the nadir and peak of glomerular E (**Figure 1C**). At 4 months, serum creatine and urine ACR values were similar among the Control, Col4α3$^{-/-}$, and TUDCA-treated Col4α3$^{-/-}$ (Col4α3^{-}

$^{/-}$-T) groups (**Figure 3**, left top two panels). However, at 7 months, when average serum creatinine and ACR were respectively 55±7 µm and 90±11, Col4α3$^{-/-}$-T values for creatine and ACR were respectively, 33±3.9 µm and 40±8.6, demonstrating reduced severity of glomerular injury in the Col4α3$^{-/-}$-T mice.

At 4 months, the value for E in the control mice was 2.1±0.04 kPa, 1.56±0.05 kPa for the Col4α3$^{-/-}$ mice, and 2.0±1.0 kPa in the Col4α3$^{-/-}$-T mice (**Figure 3C**). At 7 months, E for Control glomeruli was 2.1±0.06 kPa, and for the Col4α3$^{-/-}$ glomeruli it was 2.70±0.05 kPa, while the value for the Col4α3$^{-/-}$-T glomeruli was 1.9±0.04 kPa, a value comparable to control. These results demonstrate that TUDCA preserves the elastic properties of Col4α3$^{-/-}$ glomeruli, indicative of normalized podocyte cytoskeletal structure, mitigates the rise in serum creatinine and urine ACR in these mice and implicates UPR activation in capillary injury.

TUDCA treatment preserves Col4α3$^{-/-}$ kidney structure. Chronic kidney disease is marked by progressive fibrosis and loss of renal function, a component of which can be attributed to proteinuria(46). Our physiologic measurements at 7 months, late-stage disease, (**Figure 3A-C**) showed preserved renal function in the Col4α3$^{-/-}$-T mice implying preserved glomerular and renal structure. Low magnification kidney sections from 4-month mice stained with PAS or Picrosirius Red (PSR) show that sections from control, Col4α3$^{-/-}$, and Col4α3$^{-/-}$-T mice are indistinguishable (**Supplemental Figure S5, also see Figure 7**), indicating that at the 4 month time point, overall renal injury is minimal. At seven months (**Figure 3D**), the extent of injury in the Col4α3$^{-/-}$ kidneys is evident in the PAS and PSR-stained sections. Compared to the control kidneys, the PAS-stained Col4α3$^{-/-}$ kidneys show disrupted renal architecture, fibrosis, and inflammatory cell infiltrates. In the kidneys of Col4α3$^{-/-}$-T mice, these features are present, but to a significantly lesser extent. The insets show representative images of glomeruli from each group. The glomeruli from the Col4α3$^{-/-}$ mice are sclerotic and have excess, irregular PSR staining. Although glomeruli from the Col4α3$^{-/-}$-T mice are not normal, their structure is relatively preserved compared to the untreated Col4α3$^{-/-}$ glomeruli.

We measured the expression of genes associated with renal injury and fibrosis at 7 months using qRT-PCR of RNA samples from renal cortex in control, Col4α3$^{-/-}$, and Col4α3$^{-/-}$-T mice (**Table 1**). In Col4α3$^{-/-}$ mice, expression of Col1α1, Col1α2, Col3α1, lysyl oxidase (LOX), lysyl oxidase like 2 (Loxyl2), TGF-β1, CxCl1, Ccl2, Ccr2, CN1

(Cyr61), a gene involved in development and wound healing and repair, TNFα, and IGF2, a gene involved in hypertrophy, all increased compared to Control. In the Col4α3$^{-/-}$-T mice, the mRNA expression for these genes was reduced to levels intermediate between those in Control and untreated Col4α3$^{-/-}$ mice. The reduction of TNF-α by half by TUDCA is notable because of the role of that pathway in other renal diseases(47). EGF mRNA, a marker for renal parenchymal integrity, decreased significantly in the Col4α3$^{-/-}$ mice compared to Control, but in Col4α3$^{-/-}$-T mice, EGF mRNA was expressed at an intermediate level, significantly higher than in Col4α3$^{-/-}$ mice. At the 4 month time point, the differences between the Col4α3$^{-/-}$ mice and WT were similar to those at 7 Mo in direction, but were small and generally not statistically significant (**Supplemental Tables 1A and B**). These results demonstrate that TUDCA, initiated early in the course of disease, reduces glomerular injury and proteinuria, slows progression of nephropathy in Col4α3$^{-/-}$ mice in part by reducing cytokine and chemokine production and fibrosis, and that significant differences between the WT and col4α3$^{-/-}$ mice are only evident after 4 months when they are associated with glomerular capillary stiffening and progressive renal injury.

To correlate the light microscopic findings showing reduced disruption of renal structure in response to TUDCA with molecular parameters, we compared bulk RNAseq at 4 months in WT, Col4α3$^{-/-}$, and Col4α3$^{-/-}$-T mice. This time was chosen because it is when the course of renal disease changes with rising creatine, urine ACR, and from maximum glomerular deformability, to increasing rigidity. At 4 months, Col4α3$^{-/-}$ kidneys were enriched in genes related to extracellular matrix organization (GO:R-HAS-1474244), signaling by interleukins (R-HSA449147), mediators of inflammation, cell signaling, and cytoskeleton and adhesion (**Figure 4 and Supplemental Figure S6A**). Compared to the Col4α3$^{-/-}$ kidneys, the Col4α3$^{-/-}$-T kidneys were enriched in MAP kinase tyrosine phosphates activity, MAP kinase serine-threonine phosphatase activity, negative regulation of MAPK cascade, negative regulation of ERK1 and ERK1 cascade, and negative regulation of epithelial cell differentiation pathways **(Figure 4A and Supplemental Figure S6B)**.

We compared three groups of 4 mice, WT, Col4α3$^{-/-}$, and Col4α3$^{-/-}$-T, and identified 1346 DEGs in the WT-Col4α3$^{-/-}$ comparison, and 129 DEGs between Col4α3$^{-/-}$ and Col4α3$^{-/-}$-T mice. The top 50 increased and bottom 50 decreased genes from each comparison are shown in **Supplemental Tables 2-5**. TUDCA increased the expression of genes that inhibit the MAP kinase pathway (Dusp5, 6, 9) tyrosine kinase signaling and TGF-β-

induced EMT (Spred1, 2, Spry2), inhibit metalloproteases (TIMP3) and increased FGF10 message that promotes wound healing (FGF10) (**Figure 4B**). These effects of TUDCA may contribute to its beneficial effect on renal disease progression. The expression levels of renal injury markers, HAVCR1 (Kim1) and Lcn2 (NGAL) increased in the Col4α3$^{-/-}$ mice but had insignificant responses to TUDCA. Similarly, TUDCA did not have significant effects on genes associated with collagen or fibrosis, inflammation, or transporters (**Supplemental Figure S7**). Several other groups of genes showed interesting behavior with respect to TUDCA at 4 months. Three genes related to UPR activation were differentially expressed in the Col4α3$^{-/-}$ - Col4α3$^{-/-}$-T comparison, Xbp1 (increased 1.85 X), Dnajb9 (increased 1.50 X), and Eef1akmt3 (decreased to 0.38 X). Although tubular injury in response to proteinuria can cause UPR activation, we suspect that podocytes are the primary victims because they process mutant Col4α3,4,5 proteins, and urine protein levels are low(46, 48). The UPR signals from podocytes may be difficult to detect in bulk RNA because of the low number of podocytes compared to other cell types and episodic onset of injury. Our inability to see an effect of TUDCA on expression of the injury marker, fibrosis, and cytokine genes at 4 months while the TUDCA effects were clear at the physiologic and tissue levels and qRT-PCR for genes in treated mice at 7 months may relate to the fact that disease was relatively undeveloped at 4 months and the changes in the levels of expression of these genes were modest at that time.

TUDCA reduces podocyte loss from Col4α3$^{-/-}$ mouse glomeruli. Glomerular capillaries become deformable at 3 months, before an increase in creatine or urine ACR, indicating that podocyte injury begins at or before that point. Alport patients lose podocytes in the urine at an accelerated rate, and podocytes can be detected in their urine before significant proteinuria develops(18, 19)**.** To identify an early time point for podocyte injury, we compared glomerular podocyte density in control, Col4α3$^{-/-}$, and Col4α3$^{-/-}$-T-treated mice at 2, 3, and 4 months using WT1 staining as a podocyte marker (**Figure 5**)(49). At 2 months, before measurable reduction in glomerular E, the podocyte density was similar among all three groups (Podocytes/10^6 μm^3 ± SD, Control 296±44, Col4α3$^{-/-}$ 276±39, and Col4α3$^{-/-}$-T 262±45). At 3 months, when increased glomerular deformability was detectable in the Col4α3$^{-/-}$ glomeruli, podocyte density remained unchanged in the three groups and comparable to the values for 2 month glomeruli (Podocytes/10^6 μm^3 ± SD, Control 285±35, Col4α3$^{-/-}$ 270±40, and Col4α3$^{-/-}$ +T 299±32). In the 3 month Col4α3$^{-/-}$ mice, the SCr and ACR values were similar to those for the controls (SCr Col4α3$^{-/-}$ 12.9±0.81 vs 11.4±1.0 μM and ACR Col4α3$^{-/-}$ 0.82±0.13 vs 0.138±0.1 in Controls). However, at 4

months, we saw a clear reduction in podocyte density in the Col4α3$^{-/-}$ glomeruli, and TUDCA treatment protected glomeruli from podocyte loss (Podocytes/10^6 μm^3 ± SD, Control 276±48, Col4α3$^{-/-}$ 162±37, and Col4α3$^{-/-}$-T 246±40). At 4 months, when SCr (Col4α3$^{-/-}$ 14.8±-.67 vs Control 10.1±1.03) and urine ACR (Col4α3$^{-/-}$ 3.51±0.51 vs Control 0.059±0.02) were minimally elevated, glomerular E in the Col4α3$^{-/-}$ mice was at its lowest point, and the podocytes density in the Col4α3$^{-/-}$ glomeruli was sixty percent that of the control mice.

Early glomerular capillary deformability corresponds to reduced podocyte adhesion. Based on our findings that approximately 40% of podocytes are lost in the Col4α3$^{-/-}$ mice at 4 months (**Figure 5**), we thought that podocyte injury should be detectable at 3 months as decreased podocyte adhesion because that is the earliest detectable change in elasticity, Col4α3$^{-/-}$ podocyte numbers are preserved, and Control and Col4α3$^{-/-}$ glomeruli had similar patterns of synaptopodin and nephrin staining (**Supplemental Figure S8**). To test this possibility, we measured podocyte adhesion in 3 month-old mice as urinary podocyte loss *in vivo* in response to volume loading. Mice were injected with 0.5N saline (80 µl/g IP), and urine was collected over two hours(50). Urinary podocytes that detached and were lost into the urine were quantified by two methods, immunoblot of urine for nephrin, a podocyte-specific protein normailized for creatinine (**Figure 6A, B**), and counting WT-1 positive cells in the urine sediment (**Figure 6C**). With acute volume loading, the amount of urinary nephrin increased four-fold over control in the Col4α3$^{-/-}$ samples. TUDCA treatment reduced urine nephrin by approximately half. Urinary podocyte loss increased in Col4α3$^{-/-}$ mice compared to Control (**Figure 5C**). These observations were consistent in 3 different experiments, where although the number of total podocytes lost in the urine varied from mouse to mouse, only the Col4α3$^{-/-}$ mice consistently had multiple WT-1 positive cells in their urine. These results show that reduced podocyte adhesion and loss begin early in the course of nephropathy and suggest that early disease-associated structural alterations in podocytes including adhesion may contribute to the increased deformability of glomerular capillaries. TUDCA protects against podocyte loss at early stages of nephropathy.

TUDCA protects glomerular capillary and podocyte structure. Light microscopic images of glomeruli from 4 month old Col4α3$^{-/-}$ mice show generally preserved structure, but the glomeruli are hypertrophic compared to the WT mice and have multiple dilated capillaries (**Figure 7, top row**). Additionally, focal lesions are present,

but there is little evidence of tubulointerstitial damage. The Col4α3$^{-/-}$-T glomeruli show evidence of focal lesions and capillary dilation, but considerably less than the Col4α3$^{-/-}$ glomeruli. At 7 months, the patterns described above persist but in the Col4α3$^{-/-}$ mice are more severe. More glomerulosclerosis and focal glomerular lesions are present as well as significant tubulointerstitial injury and inflammation. The Col4α3$^{-/-}$-T kidneys show less glomerular and tubulointerstitial injury compared to the Col4α3$^{-/-}$ kidneys, but injury progressed from the 4 month time point (**Supplemental Table S6**).

We used transmission electron microscopy (TEM) to compare podocyte and GBM structures in our three groups of mice at 4 and 7 months (**Figure 8**). At 4 months, the glomeruli from the Col4α3$^{-/-}$ mice show regions of irregular GBM structure with thin and thick regions. The podocyte foot processes are normal in some regions but also show evidence of effacement and widened foot processes in other regions. Some podocyte cell bodies appear hypertrophic, exhibiting vacuolization, and have expanded ER indicative of ER stress (**Supplemental Figure S9, Supplemental Table S7**. In the Col4α3$^{-/-}$-T glomeruli, these pathologic findings are present, but less severe than in the Col4α3$^{-/-}$ mice. By 7 months, the pathologic changes in the Col4α3$^{-/-}$ GBMs and podocytes are more advanced with evidence of substantial glomerulosclerosis, and the Col4α3$^{-/-}$-T glomeruli have characteristics intermediate between the WT and Col4α3$^{-/-}$ glomeruli. The pathologic findings are quantified in **Supplemental Table 7**.

Comparison of Col4α3$^{-/-}$ mouse transcriptomic data to NEPTUNE human biopsy data. To determine the relevance of our mouse Alport Syndrome model to human disease, we performed a cross-species analysis between 7 month Col4α3$^{-/-}$ RNA samples and human RNA-seq data from micro-dissected glomeruli from biopsy samples in the NEPTUNE cohort(47). The 7 month time point in the Clo4α3$^{-/-}$ mice is the best phenotypic match for the NEPTUNE patients because both groups had significant proteinuria and many NEPTUNE patients also had elevated serum creatinine levels. Comparing 182 samples from the NEPTUNE cohort with 22,017 genes measured, we found enrichment of genes associated with proteinuria in the (IC6)(47). The top 10 % of overexpressed proteinuria associated genes in our Col4a3$^{-/-}$ model were strongly enriched in micro-dissected glomerular bulk-RNA seq data of FSGS patients with nephrotic and sub-nephrotic range proteinuria in the NEPTUNE cohort (p=1.22E-6; q=5.11E4, Odds Ratio: 2.6 (**Figure 9**)(47, 51). **Table 2** shows RT-PCR validation

of expression of selected genes gene (Lif, Krt19, C3, FosB, Vcan, and Egr1) from the NEPTUNE cohort in the 7 Month Col4α3$^{-/-}$ mouse data. Not only did these genes change in the same direction in the Col4α3$^{-/-}$ mouse data, but the increases were suppressed by TUDCA. The paper by Mariani et al showed that in patients with FSGS and MCD who progressed, TNF-α signaling pathway markers, TIMP1 and CCL2 (MCP-1) were increased in urine and renal biopsy tissue. At 7 Mo, we find that they are also increased (Ccl2 9.2 X, TIMP1 20.8 X, and TNF-α 2.91 X over WT control (base 10). TNF-α was not significantly different or not differentially expressed at 2 and 4 months, TIMP-1 increased 2.1-fold and 4-fold at 2 and 4 months, and Ccl2 was not significantly different at 2 months, but increased 2.5-fold at 4 months. These results indicate that not only does a group of genes associated with proteinuria in human renal biopsies of patients with glomerular disease mirror the Alport mouse model, but that genes that have pathologic roles in kidney glomerular disease are shared between these two datasets, and in the col4α3$^{-/-}$ mice, the magnitude of the change correlates with the stage of the disease.

Discussion.

We followed the course of nephropathy in Col4α3$^{-/-}$ mice (C57Bl6 strain) from 2 to 8 months of age to identify mechanisms of renal injury at early time points. We assessed renal function and structure as well as glomerular capillary and podocyte structure, function, and elastic properties. We have three principal findings. First, in Col4α3$^{-/-}$ mice, Alport nephropathy has two distinct phases. In the first phase, birth through 4 months, podocyte injury and loss occur in the absence of significant proteinuria, reduced renal function, or tubulointerstitial injury. Evidence of podocyte injury includes increased deformability of glomerular capillaries, reduced adhesion of podocytes to glomerular capillaries, and podocyte loss. During this period, renal genes associated with inflammation and fibrosis are activated, but not to levels sufficient to alter renal histology or function. The second phase, from 4 to 7 months, following loss of approximately 40% of podocytes, is characterized by increasing rigidity of glomerular capillaries, progressive proteinuria, decreasing excretory function, progressive glomerulosclerosis, and tubulo-interstitial fibrosis. The expression if many inflammatory mediators increases significantly during this time. The second finding is that TUDCA, an agent that reduces the consequences of UPR activation, significantly slowed progression of renal disease in Col4α3$^{-/-}$ mice. This is the first demonstration that interfering with UPR activation suppresses the Alport renal disease phenotype and implicates the UPR pathway in the pathogenesis of the disease. Third, podocyte injury occurs early in the course of nephropathy,

before proteinuria or other phenotypic changes, is characterized by increased capillary deformability and reduced podocyte adhesion to capillaries. This increased deformability probably sensitizes the capillaries to mechanical hemodynamic injury. This and other primarily glomerular diseases are likely to benefit from earlier intervention than generally occurs in clinical settings.

Podocyte injury, or hypertrophy in response to podocyte loss or other hypertrophic stimuli can cause increased capillary deformability that may represent a podocyte-specific remodeling program (10, 11, 16, 52, 53). The first observed step in podocyte injury is rearrangement of podocyte cytoskeletal structures with effacement of foot processes, ultimately leading to loss, so a difference between the biophysical properties of effaced or injured and normal podocytes is a reasonable expectation. Increased podocyte and capillary deformability may predispose to mechanical trauma and accelerate glomerular failure. This idea is consistent with the beneficial effect of ACEI/ARB therapy(54). The relevance of increased capillary deformability to the Col4α3$^{-/-}$ mouse model is evident from studies of Gyarmati et al, who found dilated glomerular capillaries with aneurisms and thrombi in early-stage Col4α5$^{-/-}$ KO mice (C57/Bl6 background), similar to our results where capillary deformability was measured directly(17). Hypertrophy appears sufficient to increase the deformability of podocytes and glomerular capillaries. Cortes et al perfused glomeruli from control and remnant rat kidneys with hypertrophic glomeruli at progressively increasing pressures over the physiologic range and calculated values for compliance. Conversion of compliance to E yields a value 2.3 kPa in control glomeruli that is similar to ours, 2.2 kPa. In the remnant kidney glomerular E decreased by 40% to approximately 1.4 kPa, a value similar to 1.6 kPa seen in our 4 month old Col4a3$^{-/-}$ mice(11, 52). These results indicate that the GBM in early Alport nephropathy is not rigid, does not determine the distensibility of glomerular capillaries, and that podocyte structure is more likely to have the dominant effect. In this setting, normal blood pressure is likely to injure podocytes and hypertension would be even more damaging. The temporal association of podocyte loss with decreased glomerular E suggests a causal relationship.

The relationship between podocyte and GBM structure, and the mechanical integrity of glomerular capillaries is not fully defined. In short-term studies where the structure of the GBM is unlikely to change, reinforcement of the actin cytoskeleton with agents such as Jasplakinolide or high Mg (increases Integrin affinity and F-actin), or

WNK1 kinase activation reduces capillary deformability(10, 11, 32, 55). Conversely, chemical disruption of the podocyte cytoskeletons with actin depolymerizing agents, protamine, WNK1 kinase inhibition, or ischemia-reperfusion injury increase deformability. These results demonstrate an essential role for podocytes in determining capillary wall mechanical properties(11, 32). Elastic environment and the mechanical behavior of neighboring cells can affect the mechanical properties of podocytes independently of the nature of the matrix(6, 10). In genetic experiments, the structure of the integrin-linked cytoskeleton can affect matrix composition by a mechanism involving recruitment of α-actinin-4 and PDLIM-5 to adhesomes by EPB41L5(24). Reduced recruitment of these proteins results in decreased adhesion strength and synthesis of matrix components, and increased recruitment has the opposite effect(8). Inflammatory injury of other glomerular cells may also contribute to podocyte injury(17). All of these factors probably contribute to aggregate tissue elastic properties and represent an integrated cellular response to injury that predisposes to mechanical injury.

We find initial increased deformability and reduced podocyte adhesion in 3 month Col4α3$^{-/-}$ glomeruli, a time when we cannot detect podocyte loss and glomeruli are normal at the light microscopic level. Podocyte injury probably begins perinatally with production of Col4α3, 4, and 5 and podocytes are exposed to protein that they cannot be processed normally. Additionally, they would be exposed to increased hemodynamic force from birth, a second insult possibly tolerated badly because of existing disordered protein processing and cytoskeletal remodeling. GO and pathway analysis covering 2 – 7 months, showed activation of pathways related to epithelial cell development, matrix structure, cell adhesion, and inflammatory signaling. At two months, GO analysis showed that extracellular matrix organization and disassembly pathways were activated as well as signaling by IL-4 and IL-13. At four months, the major active pathways in the WT – Col4α3$^{-/-}$ mouse comparison were extracellular matrix organization, inflammatory response, and cell-matrix adhesion with increased expression of matrix, adhesion, cytokine, and chemokine genes. At 7 months, the primary pathways and genes activated relate to fibrosis, inflammation, and those wit reduced expression relate to loss of differentiated functions (eg. Transporters) and represent a pattern similar to that of other late-stage renal diseases (**Figure 1D, Supp Fig S7**).

At four months, the physiologic evidence of renal injury in the Col4α3$^{-/-}$ mice was increased deformability of glomerular capillaries and podocyte loss with an abnormal GBM. Transcriptomic analysis showed activation of fibrosis, cytokine, and chemokine pathways, but despite this, renal structure and function were not degraded significantly (**Figures 1, S5, 7**). At four months, TUDCA treatment preserved glomerular capillary elasticity, podocyte number, and reduced glomerular capillary dilation, but had only a minor effect on renal transcriptomic injury markers (collagen, fibrosis, or inflammation genes) (**Supplemental Figure S7**). However, the effect of TUDCA on the renal disease phenotype in the Col4α3$^{-/-}$ mice and many of these genes at 7 months was dramatic (**Figure 3, Table 1**). Our inability to see clear effects of TUDCA on renal parenchymal injury at 4 months may relate to primary effects on podocytes and other glomerular cells in this early period, the relatively low-level of inflammatory mediators and injury at this stage compared to seven months following the development of high-grade proteinuria, and the potentially low sensitivity of the bulk RNAseq method to assess gene expression in glomerular cells.

TUDCA is considered a chemical chaperone, and the effects of TUDCA on glomeruli and podocytes appear to involve reduction of ER stress. At four months, TUDCA normalized capillary elasticity, reduced podocyte loss, resulted in milder glomerular injury based on histology and transmission electron microscopy. Its effects probably involve suppression of UPR-mediated podocyte injury (**Figures 3, 5, 6, 7, 8**). These effects are more conspicuous at 7 months where the differences between the Col4α3$^{-/-}$ and Col4α3$^{-/-}$-T mice are greater.

TUDCA appears to have effects beyond those of a chemical chaperone(26-28) Our differential expression data comparing the 4 month Col4α3$^{-/-}$ and Col4α3$^{-/-}$-T transcriptomes suggest that TUDCA also increases expression of genes that suppress Ras-MAPK, tyrosine kinase, and FGF signaling as well as TGF-β-induced epithelial-mesenchymal transformation, and actin remodeling (**Figure 4**). These effects of TUDCA may contribute to its improvement in podocyte viability and suppression of tubulo-interstitial injury in Alport nephropathy.

Despite evidence of UPR activation in cultured podocytes, glomeruli from Alport mouse models, and skin fibroblasts from patients with Alport syndrome, we are unaware of other reports showing a benefit of UPR suppression on the course of Alport nephropathy(25, 44). Several factors may contribute to this situation. First,

podocyte injury probably begins with expression of the disrupted Col4α3,4,5 heterotrimer before or near birth, long before clinical evidence of disease(41, 56). If interventions are started with the onset of "clinical" evidence of renal disease, 4 – 6 months in the Bl6 model, sufficient injury is present that renal function may not be stabilized or its rate of loss slowed. In models that progress more rapidly such as the SvJ strain or with "severe" mutations such as the Col4α5 G5X mutation, proteinuria and renal failure occur earlier, compressing the course of disease so that interventions could occur relatively late in the disease course with more severe preexisting pathology when treatment starts(22, 57). Although UPR activation in podocytes appears to be an early step in Alport nephropathy, it probably initiates other processes that have their own trajectories and treatments including endothelial injury, and fibrosis driven in part by IL-11(17, 58). TUDCA suppresses the effects of UPR activation, and in these studies preserves glomerular biophysical properties, reduces podocyte loss, tubulo-interstitial fibrosis and inflammation, proteinuria, and loss of excretory function. All of these beneficial effects may derive from improved podocyte function, but TUDCA may also have additional effects including suppression of inflammation (28, 59, 60). We find that TUDCA increases the expression of mRNAs that could suppress fibrosis, cell migration or inflammation. Future single cell studies should begin to resolve these questions.

We show correspondence between genes associated with proteinuria in the Col4α3$^{-/-}$ mice and biopsies of nephrotic and sub-nephrotic patients with FSGS from the NEPTUNE study(47). Increases or decreases in the expression of 182 genes were shared between the two databases, and we validated directionally similar changes in the Col4α3$^{-/-}$ mice using qRT-PCR for selected genes (**Figure 9B**). We also found that like FSGS and MCD, the Alport mice have a TNF-α activation signature that begins at a low level when glomeruli appear intact, and that progresses with cumulative injury. This pathway and other shared gene expression patterns suggest that there may be a generalized pathologic response to podocyte injury that among other signals, involves TNF activation. Each glomerular injury probably has unique injury mechanisms responsible for initiating the process, that then activates a general injury response pathways. Future singe cell omic studies and understanding of renal inflammatory pathways should lead to progress treating early points in glomerular diseases and lead to improved patient outcomes.

Methods.

Reagents. All fluorescent antibodies were purchased from Invitrogen. *Antibodies for immunofluorescence* **-** Col4α3: (Rat) Clone H31 97076), Chondrex, Inc.; Col4α3: (Rabbit) MBS2026491, BioSource; Bip: ab21685, Abcam; WT-1: sc-7385, Santa Cruz; Synaptopodin: sc-21537, Santa Cruz; Nephrin: AF3169, R&D Systems. *Antibodies for immunoblotting* - Bip: ab21685, Abcam; Xbp1s: sc-7160, Cell signaling, and 24868-1-AP, Proteintech; Chop: (D46F1), #5554, Cell Signaling; GAPDH: XP, #5174S, Cell signaling; β-actin – #AM4302 Invitrogen.

Mouse breeding and treatment. Col4α3$^{-/-}$ mice in the C57Bl/6J background were obtained from Jeff Miner(22). Genotyping was performed by Transnetyx. For studies, homozygous males were bred with heterozygous females to obtain Col4α3$^{-/-}$ and Col4α3$^{+/+}$ mice. KO mice were fed 0.8% TauroUrsoDeoxyCholic Acid, 3α,7β-Dihydroxy-5β-cholanoyltaurine (TUDCA) incorporated into mouse chow from the time of weaning (25-28 days old) until sacrifice (26, 27, 29, 45). TUDCA (98% purity) was from Chemimpex and was incorporated into standard mouse chow by Teklad. Normal littermates served as controls.

We measured the serum creatinine either by submandibular puncture or exsanguination at the time of sacrifice. After clotting at room temperature for 1hr and centrifugation at 2000 x g for 10min, the supernatants were transferred to new clean tubes and stored at -80 °C for further analysis. Mouse urine samples were collected from spot urine in clean empty cages and centrifuged at 400 x g for 10min. The supernatant was transferred to new clean tube and stored at -80 °C. Urine albumin concentrations were measured using a Mouse Albumin ELISA Kit (Immunology Consultants Laboratory, Inc). Serum and urine creatinine levels were measured by UTSW O'Brien Kidney Research Center Physiology Core using capillary electrophoresis. Urine albumin-to-creatinine ratios were calculated to assess the severity of albuminuria.

Podocyte adhesion was measured in vivo by injecting 0.5N saline (80 µl/g IP), and collecting urine over two hours(50). An aliquot of urine was normalized for creatinine and immunoblotted for nephrin. Another aliquot was centrifuged, the sediment attached to a slide and stained for DAPI and WT-1.

Isolation of mouse glomeruli. To isolate glomeruli, kidneys were removed from mice, placed in iced buffer, decapsulated, and dissected on ice to isolate the cortices from the medullae. The cortices were minced with a razor blade and pushed through a screen (180 µm, W.S. Tyler Co, Cleveland, OH) with a flexible metal spatula.

The minced tissue was suspended in PBS with 5.5 mM glucose and 0.3 mM pyruvate (GIBCO), filtered through a 90 µm nylon mesh (Falcon) to remove vessels and large pieces of tissue. The filtrate was collected in a 45 µm mesh nylon filter (Falcon) and contained intact glomeruli with minimal contamination (< 2%) by tubular cells(10, 11, 61). Glomeruli were maintained in DMEM with 0.1% FBS at room temperature before drug treatment, elasticity measurements or confocal imaging.

Podocyte cell line development and culture. Podocyte cell lines were derived from WT and Col4α3$^{-/-}$ primary podocyte outgrowths from glomeruli isolated from adult mice (12-16 weeks of age). Glomeruli were maintained in DMEM with 0.1% FBS at room temperature and seeded onto collagen I-coated dishes for 4-6 days to allow primary glomerular cell outgrowth. Primary podocytes were then trypsinized, filtered with 20 µm cell strainer, and re-plated for experiments or immortalization. Primary podocytes were conditionally immortalized by infection with a lentivirus expressing the temperature sensitive SV40 T antigen tsA58. Lentivirus was produced from pLenti-SV40-T-tsA58 (abm cat# LV629) as previously described (62) using the VSV envelope from pMD2.G (Addgene cat#12259, gift from Didier Trono) and the packaging plasmid pCMV delta R8.2 (Addgene cat # 12263, gift from Didier Trono). Primary glomerular outgrowths were infected for 48 hours followed by selection with puromycin (2ug/ml). Conditionally-immortalized mouse podocytes were cultured in RPMI 1640 with 10% FBS. Cells cultures were expanded at 33°C and for experiments, differentiated at 37°C for 7-10 days as previously described (63).

Animal Studies. Animal research was performed in accordance with the UT Southwestern Medical Center Animal IACUC guidelines. The research study protocol (number 2014-0078) was approved by the UT Southwestern Medical Center Animal IACUC (NIH OLAW Assurance Number A3472-01). UT Southwestern Medical Center is fully accredited by the American Association for the Assessment and Accreditation of Laboratory Care, International (AAALAC). Animals are housed and maintained in accordance with the applicable portions of the Animal Welfare Act and the Guide for the Care and Use of Laboratory Animals. Veterinary care is under the direction of a full-time veterinarian boarded by the American College of Laboratory Animal Medicine. Mice were sacrificed for experiments by first anesthetizing with Avertin and then euthanizing by exsanguination.

Kidney total RNA sample preparation for RNAseq. Kidneys from each group of mice were removed and 20 mg of cortex was processed for RNA purification. All samples were stored with RNA later in -80 °C and thawed for RNA purification. Total RNA was purified using Direct-Zol™ RNA Miniprep Plus (Zymo research) and the concentration was measured with DS-11 FX+ (Denovix). Final RNA samples were submitted for sequencing to Next Generation Sequencing Core of UTSW. Sequence analysis and results were performed by the University of Michigan Nephrotic Syndrome Study Network (NEPTUNE).

Quantitative RT-PCR. Total RNAs were purified from each group of mouse cortex part using Direct-Zol™ RNA Miniprep Plus (Zymo research) and used for reverse transcription by SuperScript III First-Strand Synthesis System (Invitrogen). Quantitative PCR was carried out with specific primers using SYBR™ Green PCR Master Mix (Applied Biosystems) and StepOnePlus™ Real-Time PCR System (Applied Biosystems). For quantitative analysis, the samples were normalized to GAPDH (Glyceraldehyde 3-phosphate dehydrogenase) gene expression using the ΔΔCT value method. Primer sequences for specific genes are below. 5,27

Col1α1 forward: 5'-GGAGAGAGCATGACCGATGG-3' , reverse: 5'-AAGTTCCGGTGTGACTCGTG-3'

Col1α2 forward: 5'-GCTGGTGTAATGGGTCCTCC-3', reverse: 5'-ATCCGATGTTGCCAGCTTCA-3'

Col3α1 forward: 5'-AGGCTGAAGGAAACAGCAA-3', Col3α1 reverse: 5'-TAGTCTCATTGCTTGCGTG-3'

Col4a3 forward: 5'-CAAAGGCATCAGGGGAATAACT-3' (aa-88, N-terminal region, 7S domain), 5'-ATTAGTGGCAGAGCTCTCG-3' (NC-1 domain), reverse: 5'-ACCCTTAGATCCGTTGCATCC-3'

Col4a4 forward: 5'-TTTGGACAGGGTACAGCTTG, reverse: 5'-TAGTGGCACACTTGGTGGAT

Col4a5 forward: 5'-CTGGAAGAATGGGTCCAGAT, reverse: 5'-GTTCCTTTGAAACCTGGGAA

LOX forward: 5'-CCGGTTACTTCCAGTACGGT-3', reverse: 5'-ATCCGCCCTATATGCTGAAC-3'

LOXL2 forward: 5'-GGAAAGCCTACAAGCCAGAG-3', reverse: 5'-GCAGATACCAGGTCCCACTT-3'

TNFα forward: 5'-ACGTCGTAGCAAACCACCA-3', reverse: 5'-TTGTCCCTTGAAGAAAACCT-3'

TGFβ-1 forward: 5'-CAGTGGCTGAACCAAGGAG-3', reverse: 5'-ATCCCGTTGATTCCAGGTG-3'

EGF forward: 5'-ATCTGACTTCATGGAGACA-3', reverse: 5'-AACTGGCTCTGTCTGCCGT-3'

Cyr61 forward: 5'-GTGAAGTGCGTCCTTGTGGACA-3', reverse: 5'- CTTGACACTGGAGCATCCTGCA-3'

GAPDH forward: 5'-CCATGGAGAAGGCTGGGG-3', reverse: 5'-CAAAGTTGTCATGGATGACC-3'

Measurement of glomerular elasticity. The elastic moduli of glomeruli isolated from 3-6 month old mice were measured using a microprobe indenter device(10, 11, 30). Briefly, a tensiometer probe (Kibron, Inc, Helsinki) with a 250 µm radius flat-bottom needle was mounted on a 3-D micromanipulator with 160 nm step size (Eppendorf, Inc) attached to a Leica inverted microscope. A glass slide containing a dilute sample of glomeruli was imaged by bright field illumination and the bottom of the probe was brought through the air-water interface until it was just above the surface of a single glomerulus of diameter approximately 60 µm. The probe was calibrated using the known surface tension of a pure water/air interface, and the stress applied to the probe as it was lowered onto the glomerulus was measured as a function of indentation depth. In principle, this deformation geometry is that of an infinite plane compressing a spherical object. The absolute values of elastic modulus can be calculated from appropriate models that require assumptions about the adherence of the glomerulus to the probe and the glass slide, whether the glomerular elasticity is modeled as a uniform sphere or an elastic shell, and other structural factors that confound calculation of the magnitude of elastic modulus from the force-indentation data alone. In all cases indentations were kept below 15 µm to avoid large strains that could damage the glomeruli. After the largest indentations, measurements were repeated at small strains to confirm that the deformations were recoverable.

Light microscopy of renal tissue. Formalin-fixed, paraffin-embedded kidney tissue was sectioned at 3 µm, and sections were stained with periodic acid-Schiff or picrosirius red stains. Stained tissue sections were examined, and digital images were collected under brightfield microscopy with an Olympus BX-80 microscope equipped with a Q-Imaging Retiga 2000R imaging system.

Immunofluorescence staining. Treated glomeruli were spun down at 5,000g for 5 min, resuspended and fixed in 4% paraformaldehyde for 30 minutes, and then washed 3x in PBS. Washed glomeruli were resuspended in PBS, 100 µl pipetted onto a slide, and attached to a coverslip overnight at 4˚C. The slide was rinsed in PBS to remove unattached glomeruli and further fixed with 4% paraformaldehyde for 1 hour at room temperature. Attached and fixed glomeruli on coverslips were then washed 3x in PBS, blocked with SEA BLOCK Blocking Buffer (PIERCE) for 40 minutes, then permeabilized with 0.5% Triton X-100 in PBS for 10 minutes. Glomeruli on coverslips were then stained using standard procedures, and imaging was performed using a Zeiss LSM 880 confocal microscope.

Confocal microscopy. Confocal imaging was performed in the Cell Biology and Imaging Core in the O'Brien Kidney Research Core, on a Zeiss LSM880 with Airyscan laser scanning microscope equipped with Plan-Apochromat 10x/0.3 NA, 20x/0.8 NA, 25x/0.8 NA and 63×/1.40 NA oil-immersion objective (ZEISS, Oberkochen, Germany). Fluorescence images were acquired using ZEN black 2.3 software with a 20x/0.8 NA or 63x/1.40 NA objective and Zeiss Immersion Oil 518F was used for the 63x/1.40 NA objective. Experiments were performed at constant room temperature. Images or regions of interest (ROIs) were further processed with ZEN 2.6 (blue edition) software.

Electron microscopy. Tissue samples were fixed with 2.5% (v/v) glutaraldehyde in 0.1M sodium cacodylate buffer (pH7.4). After three rinses with 0.1 M sodium cacodylate buffer, samples were embedded in 3% agarose and sliced into small blocks (1mm^3), rinsed with the same buffer three times and post-fixed with 1% osmium tetroxide and 0.8 % potassium ferricyanide in 0.1 M sodium cacodylate buffer for one and a half hours at room temperature. Samples were rinsed with water and then block stained with 4% uranyl acetate in 50% ethanol for two hours. They were then dehydrated with increasing concentration of ethanol, transitioned into propylene oxide, infiltrated with Embed-812 resin, and polymerized in a 60°C oven overnight. Blocks were sectioned with a diamond knife (Diatome) on a Leica Ultracut 7 ultramicrotome (Leica Microsystems) and collected onto copper grids, post stained with 2% aqueous uranyl acetate and lead citrate. Images were acquired on a JEM-1400 Plus transmission electron microscope equipped with a LaB_6 source operated at 120 kV using an AMT-BioSprint 16M CCD camera.

Bulk RNA sequencing.

The total input of 100ng RNA was used for the library preparation on each sample. The library was prepared using Illumina TruSeq RNA Library Prep Kit v2 (RS-122-2001) according to Manufacturer's protocol. This protocol allows RNA input of 100ng-1000ng. Illumina UMI barcodes were used to multiplex the libraries as per the Manufacturer's instructions. Quality and quantity of each sequencing final library were assessed using Agilent 2100 BioAnalyzer system (Agilent, CA, USA). A total of 10 nM picogreen measured library were pooled for 1.3pM loading on the sequencer. The pooled libraries were sequenced on Illumina NexSeq platform in PE75 (75 bp paired end) run with the NextSeq reagent kit v2.5 for 75 cycles. About 30-40 Million sequencing reads were generated per sample for the transcriptome analysis.

Paired end demultiplexed fastq files were generated using bcl2fastq2 (Illumina, v2.17), from NextSeq550 v2.5 reagent's bcl files. Initial quality control was performed using FastQC v0.11.8 and multiqc v1.7. Fastq files were imported batch wise, trimmed for adapter sequences followed by quality trimming using CLC Genomics Workbench (CLC Bio, v23.0.3). The imported high-quality reads were mapped against gene regions and transcripts annotated by ENSEMBL v99 hg38 using the RNA-seq Analysis tool v2.7 (CLC Genomics Workbench), only matches to the reverse strand of the genes were accepted (using the strand-specific reverse option). Differential gene expression analysis between the sample groups was done using the Differential Expression for RNA-seq tool v2.8, where the normalization method was set as TMM. Differential expression between the groups was tested using a control group, outliers were downweighed, and filter on average expression for FDR correction was enabled.

Gene expression QC, quantification, and DEG analysis. Fastq reads were aligned to the mouse genome (GENCODE Version M27) followed by a multi-step quality control process, which included assessments at the read, mapping, and dataset levels according to RNA sequencing quality control methods previously outlined (64). Gene-level expression quantification utilized HTSeq, and the resulting count data were normalized using voom. Differential gene expression analysis was performed in R using the Limma package (65). The Benjamini & Hochberg method for controlling the false discovery rate was applied as a correction factor for the adjusted p-value. Statistically significant differentially expressed genes (DEGs) were determined based on an adjusted p-value threshold of less than 0.05. All heatmaps were created using the ComplexHeatmap R package (66).

Gene module inference and association with metadata. Independent Component Analysis (ICA) was performed using the Stabilized-ica Python package (version 2.0.0) available at https://github.com/ncaptier/stabilized-ica. This analysis was applied to gene expression data, excluding the TUDCA effect group. Subsequently, the ICA component mixing matrix was correlated with metadata, revealing a significant correlation between IC6 and UCR (p-value < 0.05). The genes contributing to IC6 were identified using an arbitrary threshold value of 3 deviations from the mean of the distribution. A network analysis was then conducted on the resulting set of 253 genes (see Supplemental Figure S2).

Cross-Species Comparison. IC6 genes from Alport mice? What age/stage? Looks like 3 Mo.

Statistical analysis. Student t test and one-way analysis of variance were used to determine statistical significance.

Author contributions

JY and ZL conducted experiments, JY, ZL, OA, and IM acquired data, JY, ZL, MA, CAA, OA, IM, SE, MK, JMH, AN, ANC, and RTM analyzed data, LAB and PAJ provided critical methods and reagents, AN, ANC and RTM wrote the manuscript, all authors contributed to editing the manuscript.

Acknowledgments

The work published in this manuscript were supported by the National Institutes of Health grant numbers DK083592 (to LAB PAJ, and RTM), the Charles and Jane Pak Center for Mineral Metabolism and Clinical Research (RTM, ANC), and the NEPTUNE consortium (JN, MK, SE, MA).

References

1. Groopman EE, Marasa M, Cameron-Christie S, Petrovski S, Aggarwal VS, Milo-Rasouly H, et al. Diagnostic Utility of Exome Sequencing for Kidney Disease. *N Engl J Med.* 2019;380(2):142-51.

2. Sharif B, and Barua M. Advances in molecular diagnosis and therapeutics in nephrotic syndrome and focal and segmental glomerulosclerosis. *Curr Opin Nephrol Hypertens.* 2018;27(3):194-200.

3. Papazachariou L, Demosthenous P, Pieri M, Papagregoriou G, Stavrou C, Zavros M, et al. Frequency of COL4A3/COL4A4 mutations amongst families segregating glomerular microscopic hematuria and evidence for activation of the unfolded protein response. Focal and segmental glomerulosclerosis is a frequent development during aging. *PLoS ONE.* 2014;9(12):e115015.

4. Deltas C, Savva I, Voskarides K, Papazachariou L, and Pierides A. Carriers of Autosomal Recessive Alport Syndrome with Thin Basement Membrane Nephropathy Presenting as Focal Segmental Glomerulosclerosis in Later Life. *Nephron.* 2015;130(4):271-80.

5. Greka A, and Mundel P. Cell Biology and pathology of podocytes. *AnnRevPhysiol.* 2012;74:299-323.

6. Hu M, Azeloglu EU, Ron A, Tran-Ba KH, Calizo RC, Tavassoly I, et al. A biomimetic gelatin-based platform elicits a pro-differentiation effect on podocytes through mechanotransduction. *Sci Rep.* 2017;7:43934.

7. Rogg M, Maier JI, Van Wymersch C, Helmstädter M, Sammarco A, Lindenmeyer M, et al. α-Parvin Defines a Specific Integrin Adhesome to Maintain the Glomerular Filtration Barrier. *J Am Soc Nephrol.* 2022.

8. Maier JI, Rogg M, Helmstädter M, Sammarco A, Schilling O, Sabass B, et al. EPB41L5 controls podocyte extracellular matrix assembly by adhesome-dependent force transmission. *Cell Rep.* 2021;34(12):108883.

9. Schell C, and Huber TB. The Evolving Complexity of the Podocyte Cytoskeleton. *J Am Soc Nephrol.* 2017;28(11):3166-74.

10. Embry AE, Liu Z, Henderson JM, Byfield FJ, Liu L, Yoon J, et al. Similar Biophysical Abnormalities in Glomeruli and Podocytes from Two Distinct Models. *J Am Soc Nephrol.* 2018;29(5):1501-12.

11. Embry AE, Mohammadi H, Niu X, Liu L, Moe B, Miller-Little WA, et al. Biochemical and Cellular Determinants of Renal Glomerular Elasticity. *PLoS One.* 2016;11(12):e0167924.

12. Rinschen MM, Grahammer F, Hoppe AK, Kohli P, Hagman H, Kretz O, et al. YAP-mediated mechanotransduction determines the podocyte's response to damage. *Sci Signaling.* 2017;10:eaaf8165.

13. Ferrell N, Sandoval RM, Bian A, Campos-Bilderback SB, Molitoris BA, and Fissell WH. Shear stress is normalized in glomerular capillaries following ⅚ nephrectomy. *Am J Physiol Renal Physiol.* 2015;308(6):F588-93.

14. Wyss HM, Henderson JM, Byfield FJ, Bruggeman LA, Ding Y, Huang C, et al. Biophysical properties of normal and diseased renal glomeruli. *AmJPhysiol(Cell).* 2011;300:C397-C405.

15. Azeloglu EU, Hardy SV, Eungdamrong NJ, Chen Y, Jayaraman G, Chuang PY, et al. Interconnected network motifs control podocyte morphology and kidney function. *Sci Signal.* 2014;7(311):ra12.

16. Calizo RC, Bhattacharya S, van Hasselt JGC, Wei C, Wong JS, Wiener RJ, et al. Disruption of podocyte cytoskeletal biomechanics by dasatinib leads to nephrotoxicity. *Nat Commun.* 2019;10(1):2061.

17. Gyarmati G, Shroff UN, Izuhara A, Hou X, Da Sacco S, Sedrakyan S, et al. Intravital imaging reveals glomerular capillary distension and endothelial and immune cell activation early in Alport syndrome. *JCI Insight.* 2022;7(1).

18. Ding F, Wickman L, Wang SQ, Zhang Y, Wang F, Afshinnia F, et al. Accelerated podocyte detachment and progressive podocyte loss from glomeruli with age in Alport Syndrome. *Kidney Int.* 2017;92(6):1515-25.

19. Wickman L, Hodgin JB, Wang SQ, Afshinnia F, Kershaw D, and Wiggins RC. Podocyte Depletion in Thin GBM and Alport Syndrome. *PLoS One.* 2016;11(5):e0155255.

20. Kriz W, Hähnel B, Hosser H, Rösener S, and Waldherr R. Structural analysis of how podocytes detach from the glomerular basement membrane under hypertrophic stress. *Front Endocrinol (Lausanne).* 2014;5:207.

21. Cosgrove D, Kalluri R, Miner JH, Segal Y, and Borza DB. Chosing a mouse model to study the molecular pathobiology of Alport glomerulonephritis. *Kidney International.* 2007;71:615-8.

22. Andrews KL, Mudd JL, Li C, and Miner JH. Quantitative trait loci influence renal disease progression in a mouse model of Alport syndrome. *AmJPath.* 2002;160(2):721-30.

23. Miner JH, and Sanes JR. Molecular and functional defects in kidneys from mice lacking collagen ‡3(IV): implications for Alport syndrome. *JCell Biol.* 1996;135(5):1403-13.

24. Schell C, Rogg M, Suhm M, Helmstädter M, Sellung D, Yasuda-Yamahara M, et al. The FERM protein EPB41L5 regulates actomyosin contractility and focal adhesion formation to maintain the kidney filtration barrier. *Proc Natl Acad Sci U S A.* 2017;114(23):E4621-e30.

25. Pieri M, Stefanou C, Zavarinos A, Erguler K, Stylianou K, Lapathitis G, et al. Evidence for activation of the unfolded protein resppnse in collagen IV nephropathies. *JASN.* 2014;25:260-75.

26. Kusaczuk M. Tauroursodeoxycholate-Bile Acid with Chaperoning Activity: Molecular and Cellular Effects and Therapeutic Perspectives. *Cells.* 2019;8(12).

27. Rani S, Sreenivasaiah PK, Kim JO, Lee MY, Kang WS, Kim YS, et al. Tauroursodeoxycholic acid (TUDCA) attenuates pressure overload-induced cardiac remodeling by reducing endoplasmic reticulum stress. *PLoS One.* 2017;12(4):e0176071.

28. Panda DK, Bai X, Zhang Y, Stylianesis NA, Koromilas AE, Lipman ML, et al. SCF-SKP2 E3 ubiquitin ligase links mTORC1/ER stress/ISR with YAP activation in murine renal cystogenesis. *J Clin Invest.* 2022;132(24).

29. Uppala JK, Gani AR, and Ramaiah KVA. Chemical chaperone, TUDCA unlike PBA, mitigates protein aggregation efficiently and resists ER and non-ER stress induced HepG2 cell death. *Sci Rep.* 2017;7(1):3831.

30. Levental I, Levental KR, Klein EA, Assoian R, Miller RT, Wells RG, et al. A simple indentation device for measuring micrometer-scale tissue stiffness. *Journal of Physics: Condensed Matter.* 2010;22:191420.

31. Ge X, Zhang T, Yu X, Muwonge AN, Anandakrishnan N, Wong NJ, et al. LIM-Nebulette Reinforces Podocyte Structural Integrity by Linking Actin and Vimentin Filaments. *J Am Soc Nephrol.* 2020.

32. Liu Z, Yoon J, Wichaidit C, Jaykumar AB, Dbouk HA, Embry AE, et al. Control of Podocyte and Glomerular Capillary Wall Structure and Elasticity by WNK1 Kinase. *Front Cell Dev Biol.* 2020;8:618898.

33. Puelles VG, van der Wolde JW, Wanner N, Scheppach MW, Cullen-McEwen LA, Bork T, et al. mTOR-mediated podocyte hypertrophy regulates glomerular integrity in mice and humans. *JCI Insight.* 2019;4(18).

34. Banu K, Lin Q, Basgen JM, Planoutene M, Wei C, Reghuvaran AC, et al. AMPK mediates regulation of glomerular volume and podocyte survival. *JCI Insight.* 2021;6(19).

35. Evangelista JE, Xie Z, Marino GB, Nguyen N, Clarke DJB, and Ma'ayan A. Enrichr-KG: bridging enrichment analysis across multiple libraries. *Nucleic Acids Res.* 2023;51(W1):W168-W79.

36. Li X, Bechara R, Zhao J, McGeachy MJ, and Gaffen SL. IL-17 receptor-based signaling and implications for disease. *Nat Immunol.* 2019;20(12):1594-602.

37. Krebs CF, Reimers D, Zhao Y, Paust HJ, Bartsch P, Nuñez S, et al. Pathogen-induced tissue-resident memory T(H)17 (T(RM)17) cells amplify autoimmune kidney disease. *Sci Immunol.* 2020;5(50).

38. Allen JE. IL-4 and IL-13: Regulators and Effectors of Wound Repair. *Annu Rev Immunol.* 2023;41:229-54.

39. Kim AH, Chung JJ, Akilesh S, Koziell A, Jain S, Hodgin JB, et al. B cell-derived IL-4 acts on podocytes to induce proteinuria and foot process effacement. *JCI Insight.* 2017;2(21).

40. Lai KW, Wei CL, Tan LK, Tan PH, Chiang GS, Lee CG, et al. Overexpression of interleukin-13 induces minimal-change-like nephropathy in rats. *J Am Soc Nephrol.* 2007;18(5):1476-85.

41. Abrahamson DR, Hudson BG, Stroganova L, Borza DB, and St John PL. Cellular origins of type IV collagen networks in developing glomeruli. *J Am Soc Nephrol.* 2009;20(7):1471-9.

42. Wiseman RL, Mesgarzadeh JS, and Hendershot LM. Reshaping endoplasmic reticulum quality control through the unfolded protein response. *Mol Cell.* 2022;82(8):1477-91.

43. Marutani T, Yamamoto A, Nagai N, Kubota H, and Nagata K. Accumulation of type IV collagen in dilated ER leads to apoptosis in Hsp47-knockout mouse embryos via induction of CHOP. *J Cell Sci.* 2004;117(Pt 24):5913-22.

44. Wang D, Mohammad M, Wang Y, Tan R, Murray LS, Ricardo S, et al. The Chemical Chaperone, PBA, Reduces ER Stress and Autophagy and Increases Collagen IV α5 Expression in Cultured Fibroblasts From Men With X-Linked Alport Syndrome and Missense Mutations. *Kidney Int Rep.* 2017;2(4):739-48.

45. Lo AC, Callaerts-Vegh Z, Nunes AF, Rodrigues CMP, and D'Hooge R. Tauroursodeoxycholic acid (TUDCA) supplementation prevents cognitive impairment and amyloid deposition in APP/PS1 mice. *Neurobiology of Disease.* 2013;50:21-9.

46. Jarad G, Knutsen RH, Mecham RP, and Miner JH. Albumin contributes to kidney disease progression in Alport syndrome. *Am J Physiol Renal Physiol.* 2016;311(1):F120-30.

47. Mariani LH, Eddy S, AlAkwaa FM, McCown PJ, Harder JL, Nair V, et al. Precision nephrology identified tumor necrosis factor activation variability in minimal change disease and focal segmental glomerulosclerosis. *Kidney Int.* 2022.

48. Lindenmeyer MT, Rastaldi MP, Ikehata M, Neusser MA, Kretzler M, Cohen CD, et al. Proteinuria and hyperglycemia induce endoplasmic reticulum stress. *J Am Soc Nephrol.* 2008;19(11):2225-36.

49. Venkatareddy M, Wang S, Yang Y, Patel S, Wickman L, Nishizono R, et al. Estimating podocyte number and density using a single histologic section. *J Am Soc Nephrol.* 2014;25(5):1118-29.

50. Cervenka L, Mitchell KD, and Navar LG. Renal function in mice: effects of volume expansion and angiotensin II. *J Am Soc Nephrol.* 1999;10(12):2631-6.

51. Yoon J, Liu Z, Alaba M, Bruggeman LA, A. JP, Arana C, et al. Glomerular Elasticity and Gene Expression Patterns Define Two Phases of Alport Nephropathy. *bioRxiv.* 2024;https://biorxiv.org/cgi/content/short/2024.02.26.582201v1.

52. Cortes P, Zhao X, Riser BL, and Narins RG. Regulation of glomerular volume in normal and partially nephrectomized rats. *AmJPhysiol(Renal Physiol).* 1996;270:F356-F70.

53. Wiggins JE, Goyal M, Sanden SK, Wharram BL, Shedden KA, Misek DE, et al. Podocyte hypertrophy, "adaptation," and "decompensation" associated with glomerular enlargement and glomerulosclerosis in the aging rat: prevention by calorie restriction. *J Am Soc Nephrol.* 2005;16(10):2953-66.

54. Kashtan CE, and Gross O. Clinical practice recommendations for the diagnosis and management of Alport syndrome in children, adolescents, and young adults-an update for 2020. *Pediatr Nephrol.* 2021;36(3):711-9.

55. Wyss HM, Henderson JM, Byfield FJ, Bruggeman LA, Ding Y, Huang C, et al. Biophysical properties of normal and diseased renal glomeruli. *Am J Physiol Cell Physiol.* 2011;300(3):C397-405.

56. Desjardins M, and Bendayan M. Ontogenesis of glomerular basement membrane: structural and functional properties. *J Cell Biol.* 1991;113(3):689-700.

57. Rheault MN, Kren SM, Thielen BK, Mesa HA, Crosson JT, Thomas W, et al. Mouse model of X-linked Alport syndrome. *JASN.* 2004;15:1466-74.

58. Widjaja AA, Shekeran SG, Adami E, Ting JGW, Tan J, Viswanathan S, et al. A Neutralizing IL-11 Antibody Improves Renal Function and Increases Lifespan in a Mouse Model of Alport Syndrome. *J Am Soc Nephrol.* 2022.

59. Keestra-Gounder AM, Byndloss MX, Seyffert N, Young BM, Chávez-Arroyo A, Tsai AY, et al. NOD1 and NOD2 signalling links ER stress with inflammation. *Nature.* 2016;532(7599):394-7.

60. Wang W, Zhao J, Gui W, Sun D, Dai H, Xiao L, et al. Tauroursodeoxycholic acid inhibits intestinal inflammation and barrier disruption in mice with non-alcoholic fatty liver disease. *Br J Pharmacol.* 2018;175(3):469-84.

61. Schlondorff D. Preparation and study of isolated glomeruli. *Methods in Enzymology.* 1990;191:130-40.

62. Naldini L, Blömer U, Gallay P, Ory D, Mulligan R, Gage FH, et al. In vivo gene delivery and stable transduction of nondividing cells by a lentiviral vector. *Science.* 1996;272(5259):263-7.

63. Shankland SJ, Pippin JW, Reiser J, and Mundel P. Podocytes in culture: past, present, and future. *Kidney Int.* 2007;72(1):26-36.

64. Hong C, Eichinger F, Atta MG, Estrella MM, Fine DM, Ross MJ, et al. Viral associations with kidney disease diagnosis and altered kidney metatranscriptome by kidney function. *Kidney Int.* 2023;103(1):218-22.

65. Ritchie ME, Phipson B, Wu D, Hu Y, Law CW, Shi W, et al. limma powers differential expression analyses for RNA-sequencing and microarray studies. *Nucleic Acids Res.* 2015;43(7):e47.

66. Gu Z. Complex heatmap visualization. *iMeta.* 2022;1(3):e43.

Figures

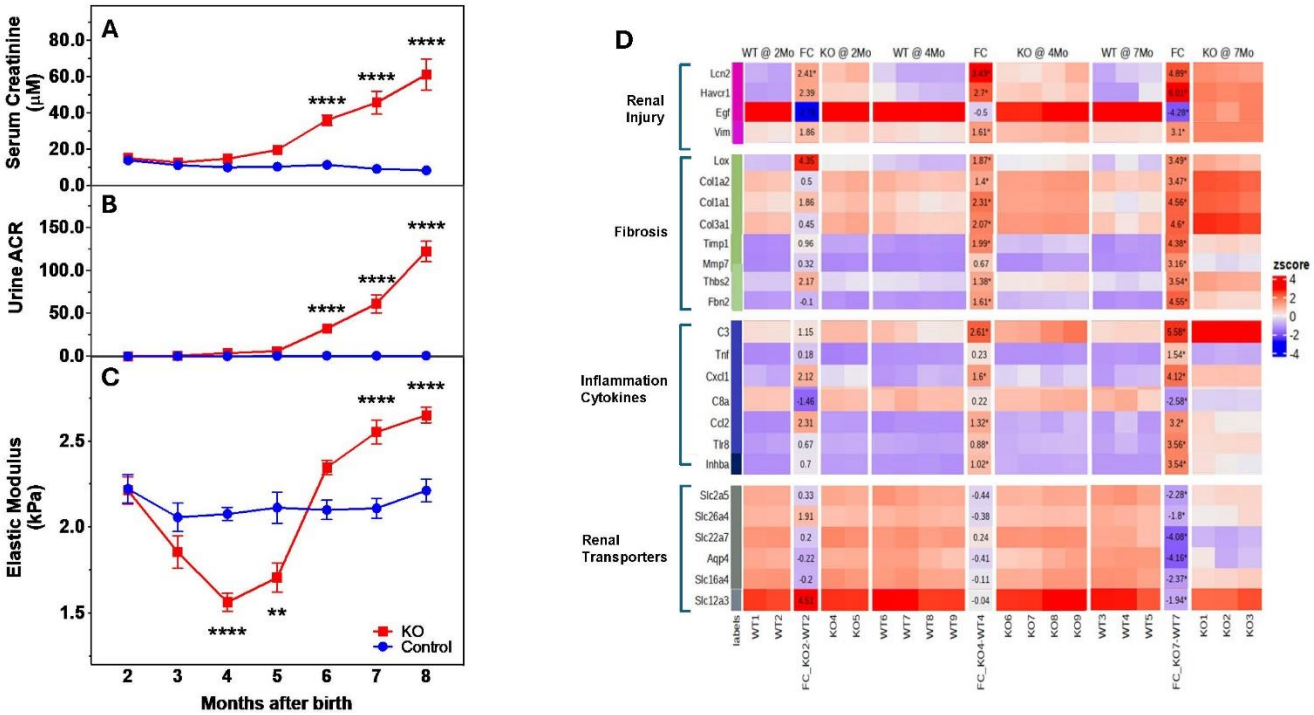

Figure 1. Measurement of serum creatinine (**A**), urine ACR (**B**), and glomerular elastic modulus (E, Young's modulus) (**C**) in Col4α3$^{-/-}$ (KO, red) mice over the course of renal disease compared to wildtype or heterozygote controls (Control, blue). Beginning two months after birth, serum creatine (µM) and urine ACR (mg/g) were measured monthly through eight months. Glomerular E (kPa) was measured in mice sacrificed at indicated time point using micro indentation of isolated glomeruli. Each point in graphs show average E values from 4 - 12 different mice. Average glomerular E for each mouse was calculated from 6-10 glomeruli. Significance was determined by 2-way ANOVA using Graphpad; **P<0.01, ****P<0.0001. **(D)** Differentially expressed genes in KO kidneys at 2, 4, and 7 months compared to age-matched Control. N=2 per group at 2 months, 4 per group at 4 months, and 3 per group at 7 months. **(E)** – has some collagen/fibrosis genes, but most are not.

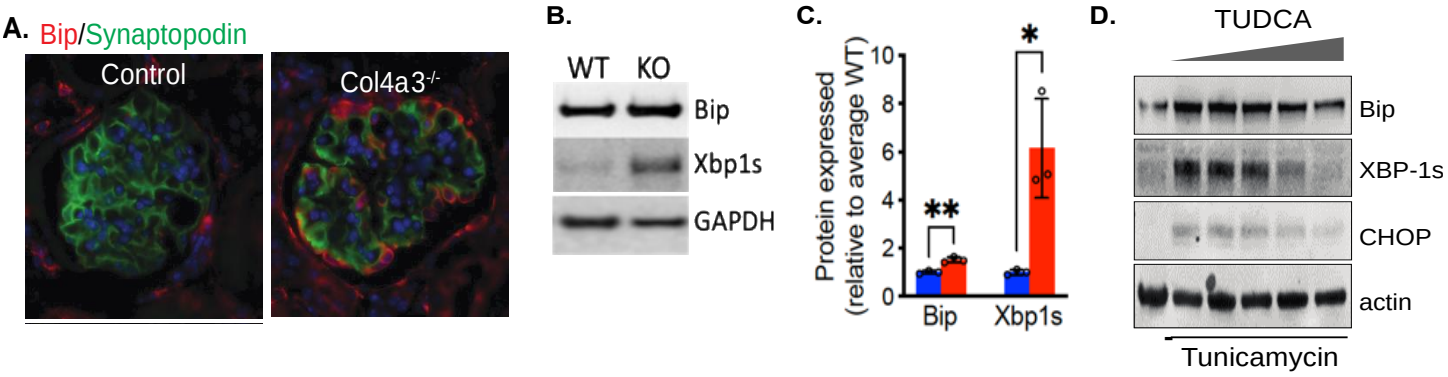

Figure 2. Evidence of UPR activation in glomeruli and podocytes from Col4α3$^{-/-}$ mice. A) IF images of Bip and synaptopodin staining in 4 month Control and Col4α3$^{-/-}$ mouse glomeruli, B) Blots of UPR markers in podocyte cell lines under basal conditions derived from WT and Col4α3$^{-/-}$ (KO) mice. The cells were maintained under standard conditions, harvested in RIPA buffer at 7% confluence, and the crude extract was immunoblotted with antibodies against bip, Xbp1s, and GAPDH. The conditionally immortalized WT and Col4α3$^{-/-}$ cells were developed from primary cultures of 3 month WT and Col4α3$^{-/-}$ glomeruli. C) Comparison of Bip and Xbp1s protein expression from B (N=3, normalized to WT). D) Efficacy of TUDCA for blocking tunicamycin-induced of UPR marker expression in WT podocytes. Podocytes were treated with tunicamycin 1 μg/ml and then increasing concentrations of TUDCA from 1 - 4 mM for four hours.

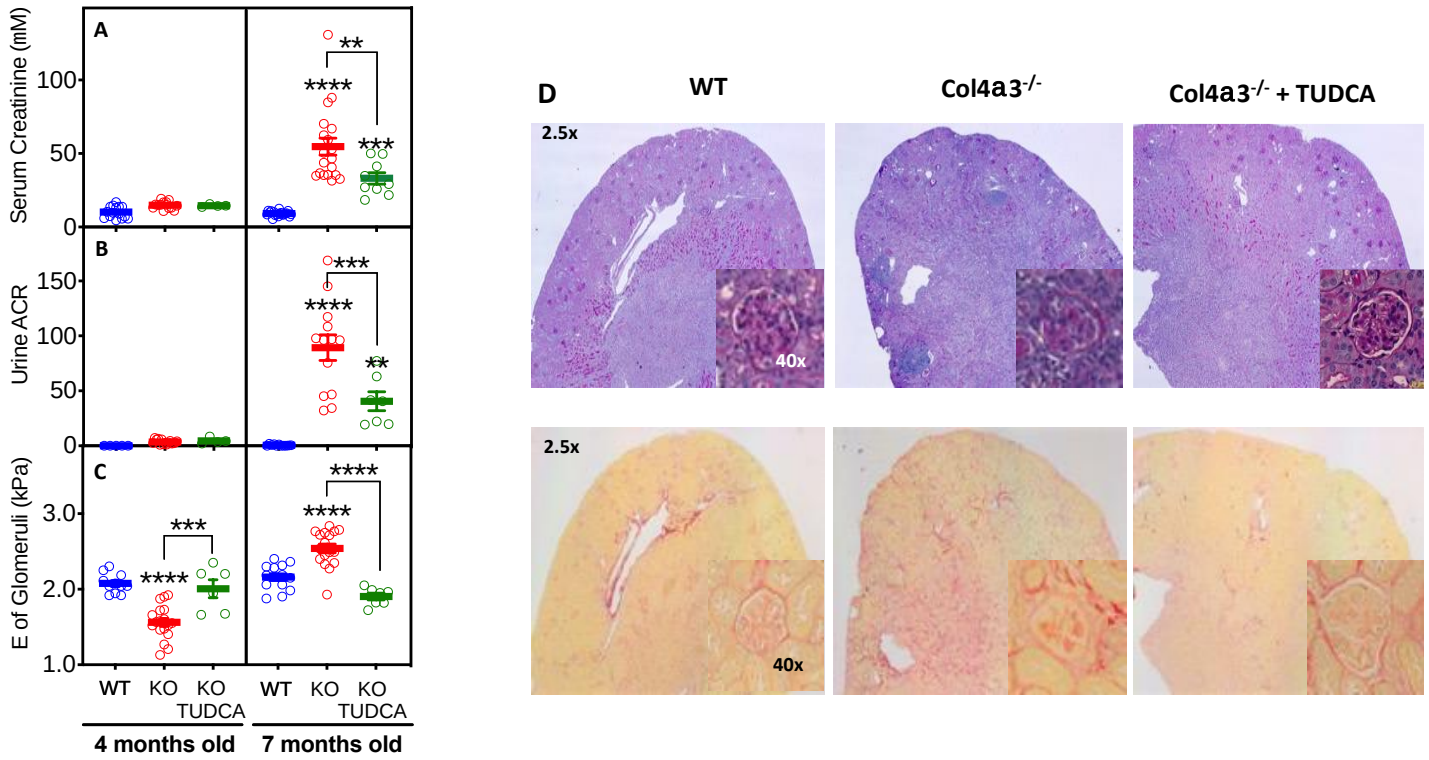

Figure 3. TUDCA treatment slows progression of renal disease and attenuates the decrease in E in Col4α3$^{-/-}$ mice. KO mice were treated from weaning (approximately 4 weeks), with 0.8% TUDCA mouse chow. **2A.** At 4 and 7 months of age, serum creatine (µM), urine ACR, and glomerular elastic modulus (E, kPa) was measured in Control, KO and TUDCA treated KO animals. Each circle represents the average of 6-10 independent E of glomeruli from a distinct mouse. Significance was determined by ANOVA and multiple comparisons test using GraphPad; **P<0.01,***P<0.001, ****P<0.0001. **2B.** Comparison of kidney cortex from Control, KO, and TUDCA treated KO animals. A) Histopathology of mouse kidney sections at 7 months of age as indicated.

Table 1A.

Fibrosis	WT (N)	KO (N)	KO-TUDCA (N)
Col1α1	1	55.5 ± 13 (3)	26.2± 6.2 (4)
Col1α2	1	29.6 ± 7.3 (5)	13.9 ± 3.2 (4)
Col3α1	1	74.1 ± 31.9 (5)	31.9 ± 2.4 (4)
Lox	1	29.7 ± 7.4 (3)	13..3 ± 7.6 (4)
Loxl2	1	21.5 ± 7.1 (3)	6.7 ± 3.1 (4)
Cytokines	1		
TGF-β1	1	4.8 ± 0.8 (4)	3.0 ± 0.7 (4)
TNF-α	1	30.3 ± 7.9 (3)	14.3 ± 3.0 (4)
IGF-1	1	9.81 ± 2.23 (4)	5.93 ± 1.72 (4)
Chemokines/Receptors			
Cxcl1	1	45.0 ± 11.4 (4)	20.9 ± 2.11 (3)
Ccl2	1	41.5 ± 9.3 (4)	34.6 ± 5.68 (4)
Ccr2	1	15.0 ± 3.45 (5)	4.04 ± 1.57 (3)
Injury Markers			
EGF	1	0.20 ± 0.1 (5)	0.7 ± 0.2 (4)
Ccn1 (Cyr61)	1	4.46 ± 0.6 (3)	2.0 ± 1.0 (4)

Table 1. Summary of qRT-PCR of selected fibrosis, cytokine, chemokine, or injury-related genes in 7 months old Col4α3$^{-/-}$ mice with and without TUDCA treatment compared to age-matched WT littermates. All values in KO and KO-TUDCA groups represent fold change from WT ± SD, and were significantly different from Control, as determined by ANOVA.

A.

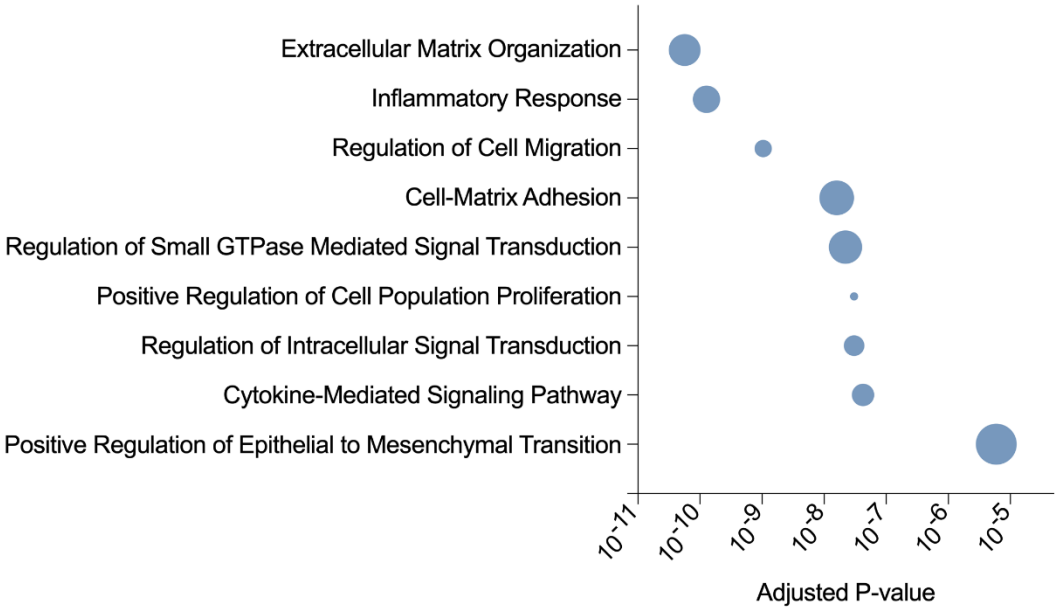

B.

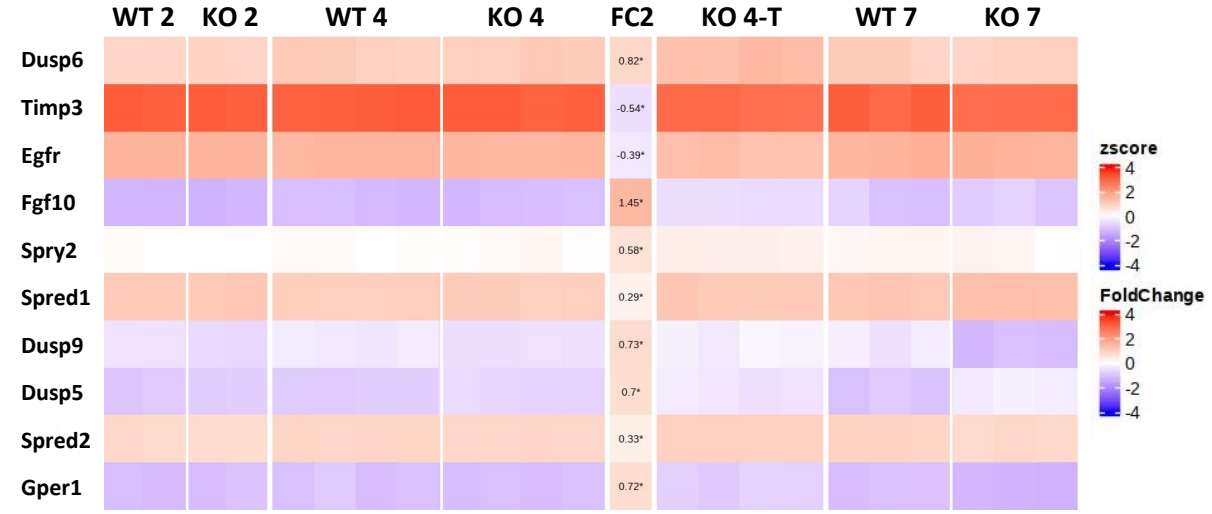

Figure 4. A) Summary of Gene Ontology categories that are over-represented by DEGs from 4 month old WT and KO PE-75 RNAseq comparison assembled by ENRICHR. B) Heatmap of genes related to ERK signaling pathway identified from KO and KO-T DEGs. The heatmap shows the samples across the top, WT and Col4α3$^{-/-}$ (KO) at 2 months (2 samples each), WT and KO 4 months (four samples each) and Col4α3$^{-/-}$ + TUDCA (KO-T) 4 months with four samples, and WT and KO at 7 months each with three samples. The column under FC shows the direction and magnitude of expression change from KO to KO-T, and * denotes significance <0.05 (Complex Heatmap R Package).

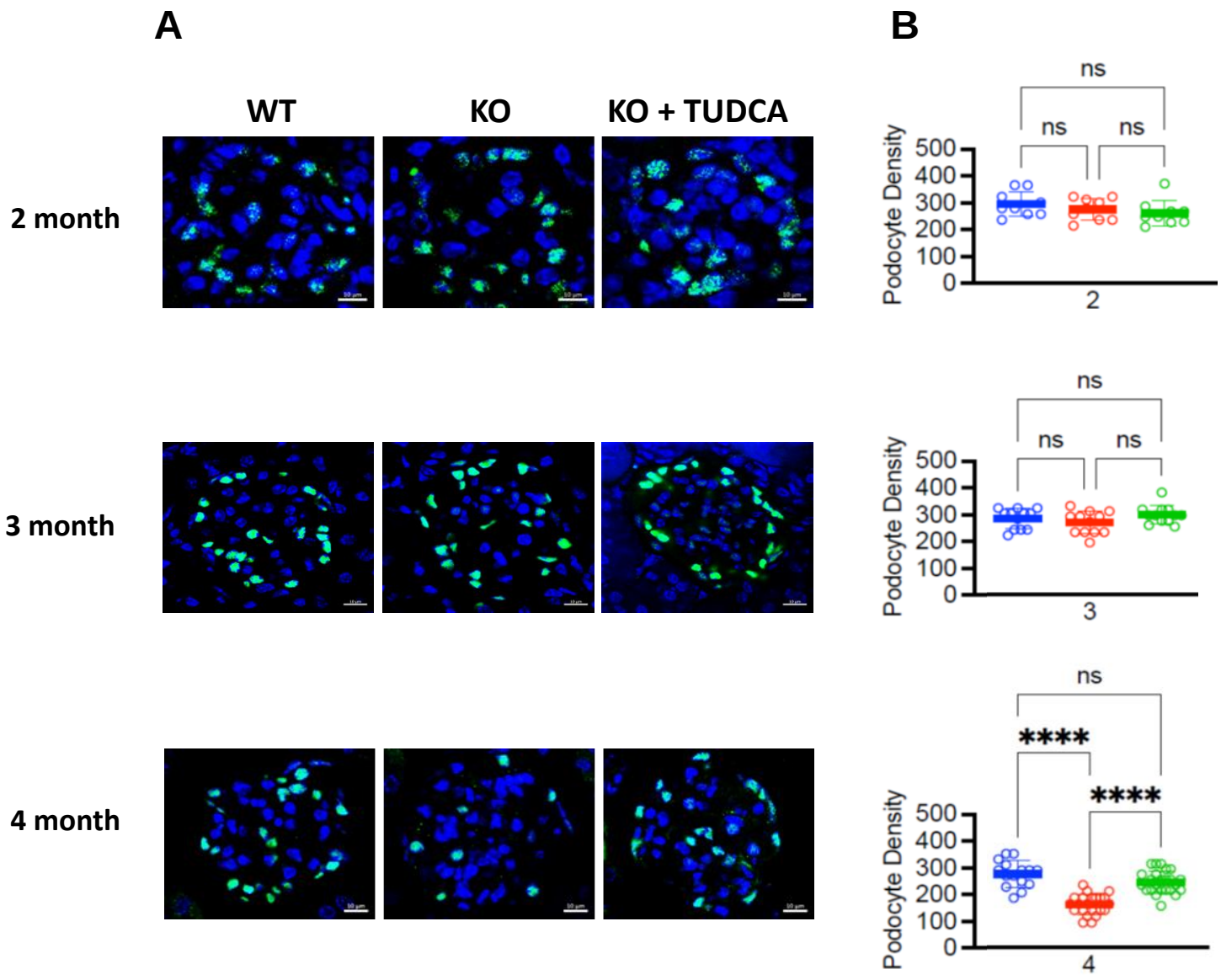

Figure 5. TUDCA reduces podocyte loss from Col4α3$^{-/-}$ mouse glomeruli. A) Representative glomeruli in kidney sections from Control, Col4α3$^{-/-}$, and TUDCA-treated Col4α3$^{-/-}$ mice from 2, 3, and 4 month old mice were stained for WT-1 and DAPI. Scale bar: 10 μm. **B)** Summary of podocyte density analysis. The number of WT-1 and DAPI-positive nuclei in 20 glomeruli from 3 mice were counted and used for podocyte density calculations. Each dot represents the number of WT-1 positive nuclei in a single glomerulus. Data are shown as mean ± SEM and significance was determined by ordinary one-way ANOVA, followed by Dunnett's multiple comparisons test; ****P<0.0001. At 2 months - Podocytes/10^6 μm^3 ± SD, Control 296±44, Col4α3$^{-/-}$ 276±39, and Col4α3$^{-/-}$+T 262±45). At 3 months - Podocytes/10^6 μm^3 ± SD, Control 285±35, Col4α3$^{-/-}$ 270±40, and Col4α3$^{-/-}$+T 299±32). At 4 months, Podocytes/10^6 μm^3 ± SD, WT 276±48, Col4α3$^{-/-}$ 162±37, and Col4α3$^{-/-}$+T 246±40).

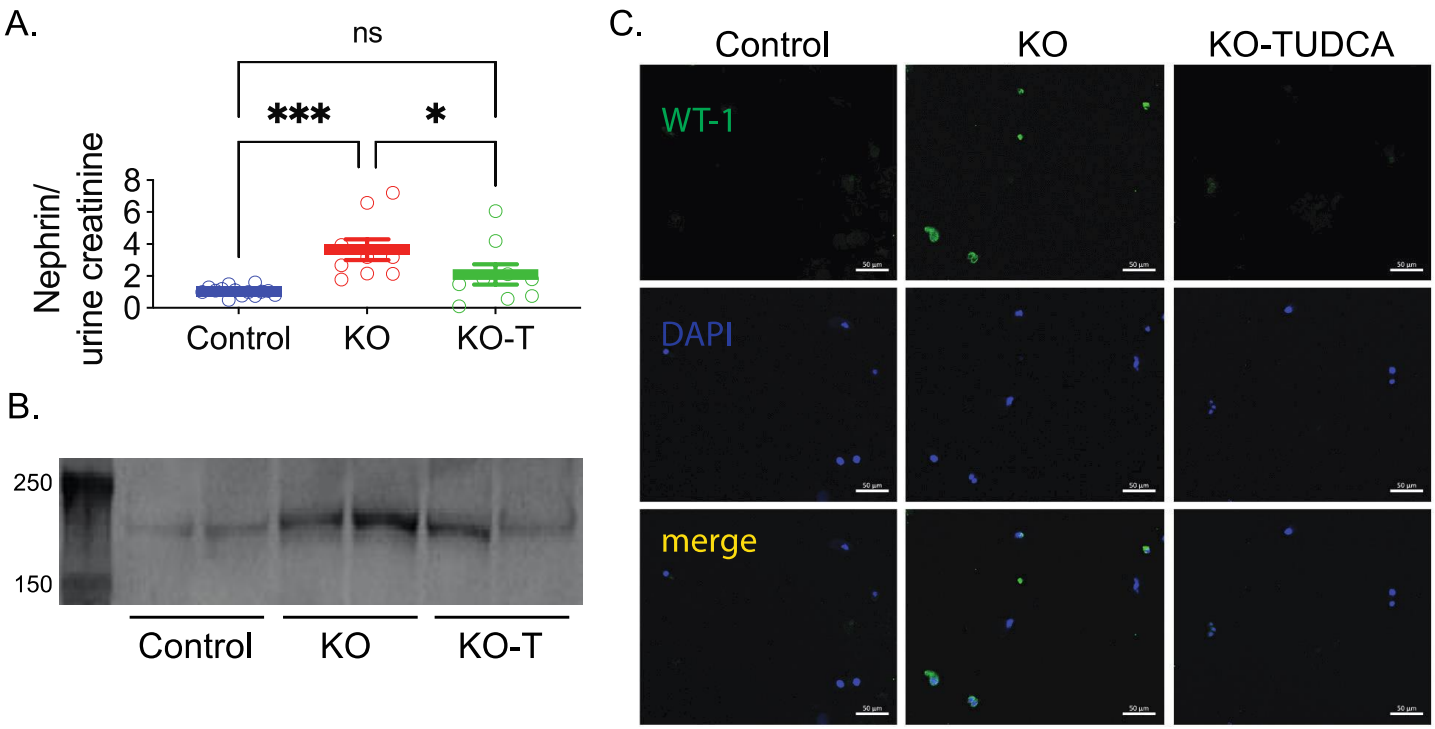

Figure 6. Glomerular capillary deformability and podocytes adhesion. Control, KO, and TUDCA-treated KO mice were injected (IP) with approximately 1 ml of saline, and urine was collected over the subsequent two hours. The urine samples were normalized for creatinine, immunoblotted for nephrin, and quantitated with densitometry. The pellet was stained for WT-1 and DAPI. A) shows aggregate data for all samples groups expressed as nephrin/creatinine (arbitrary densitometry units for nephrin) for each sample group. Each point represents a sample from a single mouse, bar indicates mean ± SEM. Significance was determined by ordinary one-way ANOVA, followed by Tukey's multiple comparisons test; *P<0.05, ***P<0.001. B) Summary data for urine nephrin immunoblot C. Representative nephrin immunoblot showing duplicate samples from each group, and C. showing representative urine sediment samples stained for WT-1 and DAPI.

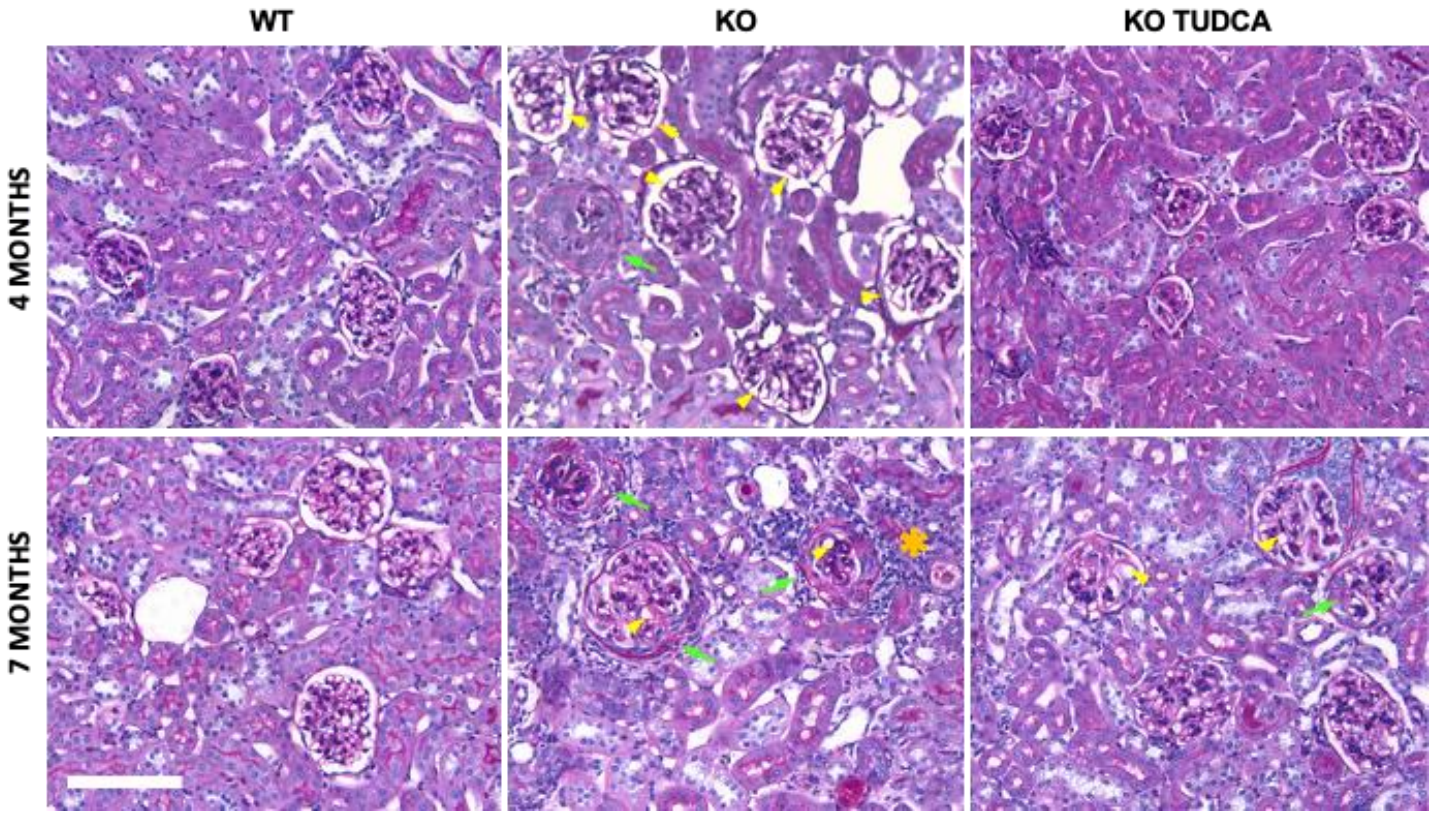

Figure 7. Brightfield photomicrographs of PAS-stained kidney sections kidneys from 4 months (top row) and 7 months old Control mice, Col4α3$^{-/-}$ (KO), and TUDCA-treated Col4α3$^{-/-}$ (KO TUDCA) mice. The 4 month KO image shows glomerular enlargement and focal proliferative glomerular lesions (green arrow), and distension of glomerular capillary lumens (yellow arrowheads) that are not observed in Control (top left) or the TUDCA treated KO mice (top right). The 7 month KO mice (bottom center) show more extensive glomerular proliferative lesion development (green arrows), with proliferation composed predominantly of epithelial cells filling Bowman's space, along with patchy areas of tubular atrophy and interstitial fibrosis and chronic inflammation (orange asterisk). The section from the 7 month TUDCA-treated mice show evidence of glomerular injury with PAS stain; bar = 200 µm for all images.

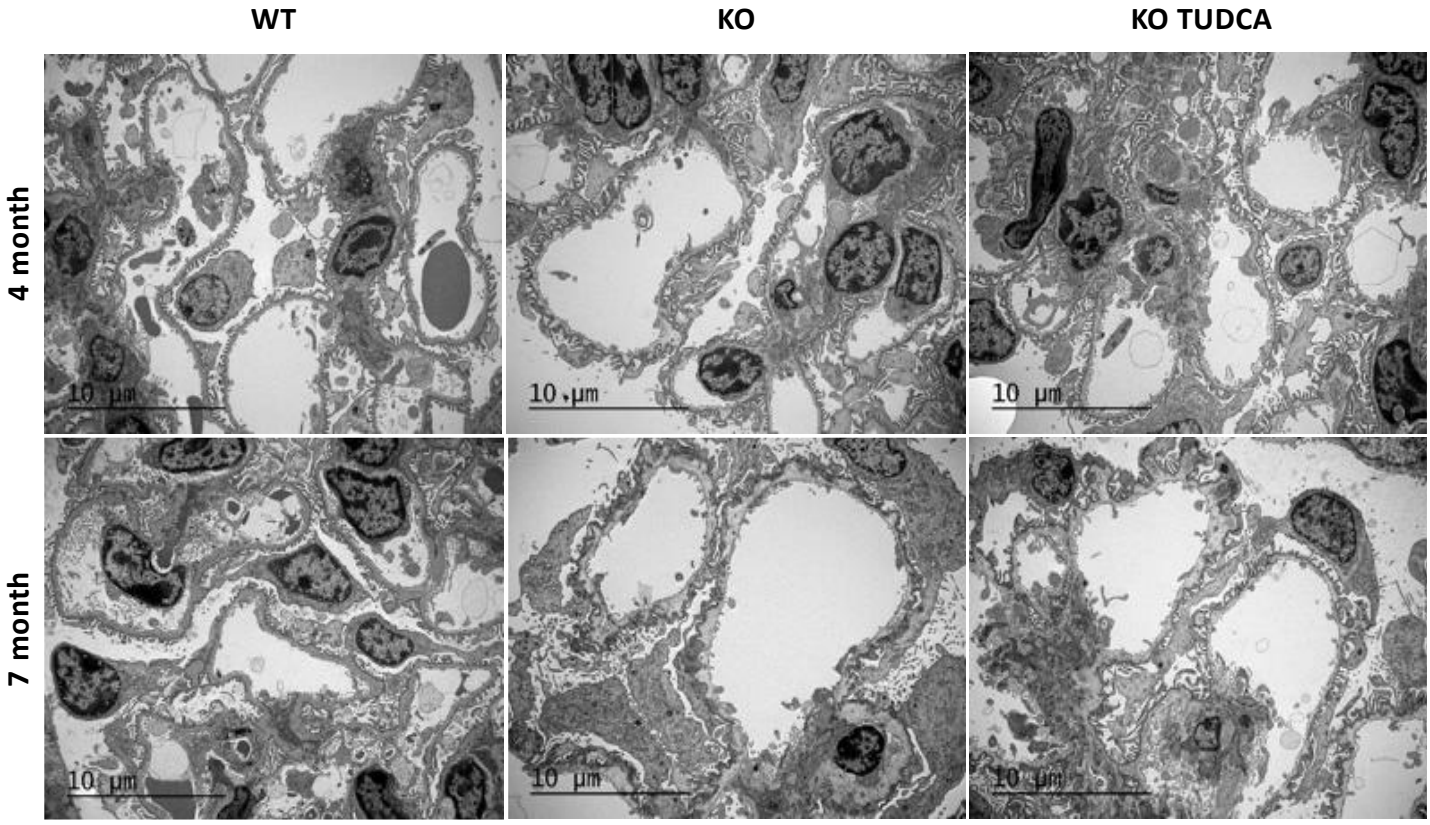

Figure 8. Transmission Electron micrographs of mouse kidneys, showing glomerular changes at 4 (top row) and 7 (bottom row) months in Control, Col4α3$^{-/-}$ (KO), and TUDCA-treated Col4α3$^{-/-}$ (KO TUDCA) mice. At 4 months, glomeruli of KO mice (top center) and KO TUDCA mice (top right) reveal features of segmental podocyte injury, including mild segmental podocyte foot process effacement, more extensive but segmental foot process irregularity, and mild microvillous change. These podocyte changes are concurrent with segmentally prominent "knob-like" subepithelial basement redundancy, characteristic of the Col4α3 -/- mouse model. Control mice (top left) show none of these changes. At 7 months (bottom row), KO mice (bottom center) reveal more severe and widespread podocyte injury, demonstrated by extensive podocyte foot process effacement and irregularity, cellular hypertrophy, and microvillous change. There are also comparable glomerular basement membrane changes including extensive subepithelial basement redundancy and segmental "basket weaving", and segmental glomerular capillary loop dilation. In contrast, KO TUDCA mice (bottom right) show podocyte and glomerular basement membrane changes that are similar in nature to those of the KO mice but are less extensive and more segmental. None of these changes are seen in Control mice (bottom left). All images are the same magnification – scale bar = 10 µm.

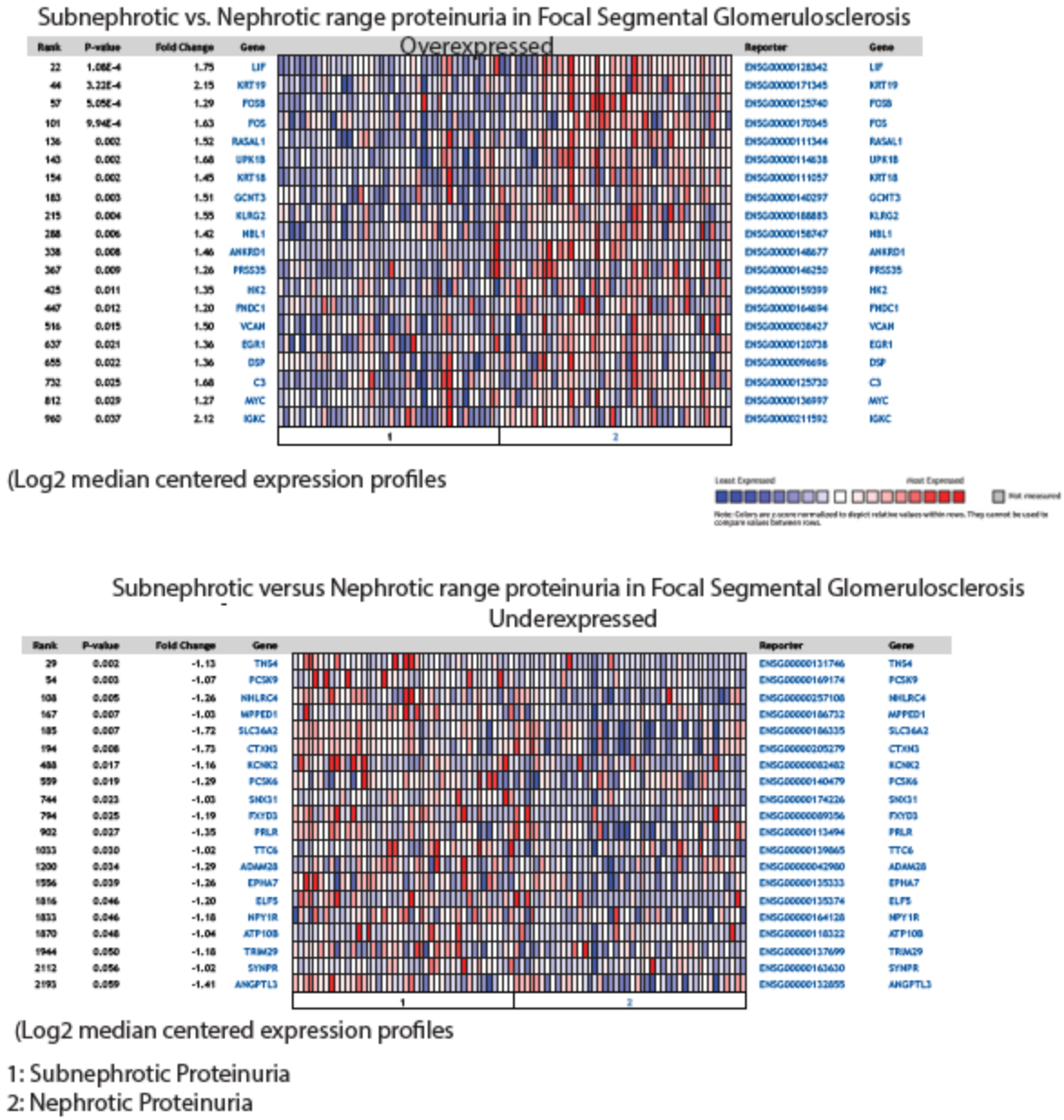

Figure 9. Comparison of *Col4a3*$^{-/-}$ proteinuria-associated genes with a human NEPTUNE FSGS cohort. Proteinuria-associated genes (IC6) were compared to scRNAseq data from isolated glomeruli from 182 patients in the NEPTUNE FSGS cohort who had either sub-nephrotic or nephrotic proteinuria, and the top 10% of over- (20) and under-expressed (20) genes are shown in A and B respectively. Group 1 represents sub-nephrotic patients and group 2 represents nephrotic patients.

Gene	WT (N)	KO (N)	KO+TUDCA (N)
Lif	**1 (5)**	**62 ± 7.91***** (5)**	**4.35 ± 0.74 (3)**
Krt19	**1 (5)**	**24.2 ± 15.6** (5)**	**6.14 ± 6.14^{+} (4)**
C3	**1 (5)**	**99.6 ± 43.7** (5)**	**17.5 ± 1.91^{++} (3)**
FosB	**1 (4)**	**19.6 ± 7.32** (3)**	**6.79 ± 1.95^{+} (3)**
Vcan	**1 (5)**	**33.4 ± 13*** (5)**	**11.34 ± 7.49^{++} (4)**
Egr1	**1 (5)**	**37.2 ± 16.6** (3)**	**14.8 ± 7.37^{+} (5)**

Table 2. Validation of selected proteinuria-associated genes from the NEPTUNE Cohort in the Col4α3$^{-/-}$ mouse data at 7 Mo. Summary of qRT-PCR of selected genes in 7 month old Col4α3$^{-/-}$ mice with and without TUDCA treatment compared to age-matched WT littermates. All values in KO and KO-TUDCA groups represent fold change from WT control (base 10) and were significantly different from WT as determined by ANOVA (* $p<0.05$, ** $P<0.01$, *** $P<0.001$, **** $p<0.0001$ for KO vs WT, and $^{+}$ $p<0.05$, $^{++}$ $P<0.01$, for KO vs KO+TUDCA.